9-11-2017

Solar Cell with PbS Quantum Dots Sensitized TiO 2 -Multiwalled Carbon Nanotubes Composite, Sulfide-titania gel and Tin Sulfide Coated C-fabric

Ramesh K. Kokal

Melepurath Deepa

Ankarao Kalluri

Shrishti Singh

Isaac Macwan

Fairfield University, imacwan@fairfield.edu

Prabir K. Patra

Jeff Gilarde

See next page for additional authors

Peer Reviewed

Published Citation

Kokal, Ramesh K., Melepurath Deepa, Ankarao Kalluri, Shrishti Singh, Isaac Macwan, Prabir K. Patra and Jeff Gilarde. “Solar Cells with PbS Quantum Dot Sensitized TiO 2 –multiwalled Carbon Nanotube Composites, Sulfide-Titania Gel and Tin Sulfide Coated C-Fabric.” Physical Chemistry Chemical Physics. 19, no. 38 (2017): 26330-26345. https://doi.org/10.1039/C7CP05582J.

PCCP

Effects of Carbon Nanotubes in Photoanode, Tin Sulfide in Counter Electrode and Titania in Electrolyte on Quantum Dot Solar Cell Performance

Journal:	*Physical Chemistry Chemical Physics*
Manuscript ID	CP-ART-05-2017-003498
Article Type:	Paper
Date Submitted by the Author:	24-May-2017
Complete List of Authors:	Kokal, Ramesh Kumar; Indian Institute of Technology Hyderabad, Department of Chemistry Deepa, Melepurath; Indian Institute of Technology, Department of Chemistry Kalluri, Ankarao ; University of Bridgeport Singh, Shristhi ; University of Bridgeport Macwan, Isaac ; University of Bridgeport Patra, Prabir; University of Bridgeport, Mechanical Engineering Gilarde, Jeff ; Wesleyan University

Article type: Full paper

Website www.rsc.org/pccp
Impact factor* 4.449

Journal expectations To be suitable for publication in *Physical Chemistry Chemical Physics* (*PCCP*) articles must include significant new insight into physical chemistry.

Article type: Full paper Original scientific work that has not been published previously. Full papers do not have a page limit and should be appropriate in length for scientific content.

Journal scope Visit the *PCCP* website for additional details of the journal scope and expectations.

PCCP is an international journal for the publication of cutting-edge original work in physical chemistry, chemical physics and biophysical chemistry. To be suitable for publication in *PCCP*, articles must include significant new insight into physical chemistry; this is the most important criterion that reviewers should judge against when evaluating submissions. Example topics within the journal's broad scope include:

- Spectroscopy
- Dynamics
- Kinetics
- Statistical mechanics
- Thermodynamics
- Electrochemistry
- Catalysis
- Surface science
- Quantum mechanics
- Theoretical research

Interdisciplinary research areas such as polymers and soft matter, materials, nanoscience, surfaces/interfaces, and biophysical chemistry are also welcomed if they demonstrate significant new insight into physical chemistry.

Reviewer responsibilities Visit the Reviewer responsibilities website for additional details of the reviewing policy and procedure for Royal of Society of Chemistry journals.

When preparing your report, please:

- Focus on the originality, importance, impact and reliability of the science. English language and grammatical errors do not need to be discussed in detail, except where it impedes scientific understanding.
- Use the journal scope and expectations to assess the manuscript's suitability for publication in *PCCP.*
- State clearly whether you think the article should be accepted or rejected and include details of how the science presented in the article corresponds to publication criteria.
- Inform the Editor if there is a conflict of interest, a significant part of the work you cannot review with confidence or if parts of the work have previously been published.

Thank you for evaluating this manuscript, your advice as a reviewer for *PCCP* is greatly appreciated.

Dr Anna Simpson Executive Editor
Royal Society of Chemistry, UK

Professor Seong Keun Kim Editorial Board Chair
Seoul National University, South Korea

**2015 Journal Citation Reports®, (Thomson Reuters, 2016)*

भारतीय प्रौद्योगिकी संस्थान हैदराबाद
Indian Institute of Technology Hyderabad

Indian Institute of Technology Hyderabad
Kandi – 502 285, Sangareddy, Telangana, INDIA
Phone: (040) 2301 6033; Fax: (040) 2301 6003 /32

MD/IITH/Chem/LA1 24th May 2017

Prof Seong Keun Kim
Chair, Editorial Board
Physical Chemistry Chemical Physics
RSC Publications

Subj: Submission of a manuscript to "**Physical Chemistry Chemical Physics**"

Dear Prof. Kim,

We hereby submit our manuscript entitled "Effects of Carbon Nanotubes in Photoanode, Tin Sulfide in Counter Electrode and Titania in Electrolyte on Quantum Dot Solar Cell Performance" by Ramesh K Kokal et al., for considering the same for publication in "Physical Chemistry Chemical Physics".

The statement describing the manuscript's significance in terms of new physical chemistry insights and the impact this MS is provided below.

The trajectory of power conversion efficiencies (PCEs) of quantum dot solar cells (QDSCs), has been nothing short of spectacular, especially over the last three years. Liquid junction QDSCs with efficiencies greater than 11% have been demonstrated successfully, thus giving a stiff competition to DSSCs. Quasi-solid state QDSCs with high efficiencies are therefore very much desirable for taking them to the next level. The charge transfer phenomena at the multiple interfaces in QDSCs essentially control their PCEs. In this study, a gel electrolyte with poly(vinyl alcohol) as a gelatinizing agent and TiO_2 nanoparticles as a filler cum passivating layer has been used for the first time. Another worrisome issue with regard to most of the high efficiency QDSCs reported in literature, is the widespread use of cadmium based QDs, which are exceedingly toxic. In comparison, lead chalcogenides (e.g. PbS) are less toxic, and also allow a broad spectral conversion spanning from visible to near infrared region due to a narrow band gap of around 1 eV. Besides making appropriate choices for the electrolyte, and the photosensitizer, another important component of a QDSC is the counter electrode (CE), which ideally should be cheap and highly catalytic, and easy to fabricate. Here, again for the first time, a SnS/C-fabric electrode with a high catalytic activity was applied to QDSCs, where low cost tin sulfide (SnS) NPs were anchored to carbon (C)-fabric. The wide band gap semiconductor, the widely used TiO_2 at the photoanode, was also modified by replacing it with a hydrothermally synthesized TiO_2-multiwalled carbon nanotubes (MWCNTs) composite, to improve its' charge transport characteristics.

All the above described design strategies cumulatively improve the interfacial characteristics of the cell and result in a quasi-solid-state QDSC, with a heretofore unreported configuration of TiO_2-MWCNTs/PbS/ZnS-Gel (with PVA, S^{2-}, TiO_2 NPs)-SnS/C-fabric that delivers a PCE of 6.3% (for champion cell). Detailed analysis shows that (i) MWCNTs enable fast electron transport, and reduce electron recombination, (ii) TiO_2 NPs in the electrolyte also suppress recombination, and (iii) SnS/C-fabric shows excellent catalytic activity towards polysulfide reduction, and high conductance as well that allows fast electron injection into the electrolyte during cell operation. These factors work in tandem to produce a cell that gives a high open circuit voltage and a large short circuit current density, which maximize the cell efficiency.

The approaches used in this study are scalable, and therefore can be easily applied for the development of practical large area cells. We believe this study will be of great scientific interest to researchers

working in QDSCs and DSSCs, particularly with the view of developing cells with reproducible performances.

We look forward to contributing to your Journal.

Thanking you
Sincerely

Melepurath Deepa
Associate Professor
Department of Chemistry, IIT Hyderabad, India

Journal Name

ARTICLE

Effects of Carbon Nanotubes in Photoanode, Tin Sulfide in Counter Electrode and Titania in Electrolyte on Quantum Dot Solar Cell Performance

Received 00th January 20xx,
Accepted 00th January 20xx

DOI: 10.1039/x0xx00000x

www.rsc.org/

Ramesh K. Kokal,[a] Melepurath Deepa,[a,*] Ankarao Kalluri,[b] Shristhi Singh,[b] Isaac Macwan,[b] Prabir K Patra,[b,c] Jeff Gilarde[d]

Novel approaches to boost quantum dot solar cell (QDSC) efficiencies are in demand. Here, three strategies are used: (i) use of a hydrothermally synthesized TiO_2-multiwalled carbon nanotubes (MWCNTs) composite instead of conventional TiO_2, (ii) use of a counter electrode (CE) that has not been applied to QDSCs till date, namely, tin sulfide (SnS) nanoparticles (NPs) coated over a conductive carbon (C)-fabric, and (iii) use of a quasi-solid-state gel electrolyte composed of S^{2-}, an inert polymer and TiO_2 nanoparticles as opposed to a polysulfide solution based hole transport layer. MWCNTs by the virtue of their high electrical conductivity and a suitably positioned Fermi level (below the conduction bands of TiO_2 and PbS) allow fast photogenerated electron injection to the external circuit, and this is confirmed by the higher efficiency of 6.3% achieved for a TiO_2-MWCNTs/PbS/ZnS based (champion) cell, compared to the corresponding TiO_2/PbS/ZnS based cell (4.45%). Nanoscale current map analysis of TiO_2 and TiO_2-MWCNTs reveal the presence of narrowly spaced highly conducting domains in the latter, which equips it with an average current carrying capability greater by a few orders of magnitude. Electron transport and recombination resistances are lower and higher respectively for the TiO_2-MWCNTs/PbS/ZnS cell relative to the TiO_2/PbS/ZnS cell, thus leading to a high performance cell. The efficacy of SnS/C-fabric as a CE is confirmed from the higher efficiency achieved in cells with this CE compared to C-fabric based cells. Lower charge transfer and diffusional resistances, slower photovoltage decay, high electrical conductance and lower redox potential impart high catalytic activity to the SnS/C-fabric assembly for sulfide reduction and thus endow the TiO_2-MWCNTs/PbS/ZnS cell with a high open circuit voltage (0.9 V) and a large short circuit current density (~20 mA cm^{-2}). This study attempts to unravel how simple strategies can amplify QDSC performances.

Introduction

Quantum dot solar cell (QDSC) efficiencies, are at present almost as high as the power conversion efficiencies (PCEs) achieved in dye sensitized solar cells (DSSCs), greater than 11%. [1] Compared to dyes in DSSCs, QDs are relatively less costly, are easy to process under non-inert conditions at low temperatures, and offer other benefits such as multiple exciton generation (the ability of a QD to produce more than one electron per impinging photon), air-stability, and panoramic solar spectrum harvesting by judicious choice of the dot. [1-5] QDSC technology has now reached a stage, where the semiconducting oxide/QD/electrolyte- and counter electrode/current collector- interfaces can be carefully designed and implemented to maximize PCEs and minimize recombination losses.

Of the various components in a QDSC, firstly, the wide band gap semiconducting scaffold (such as TiO_2), can be transformed to a more efficient electron acceptor, by making a composite with an electron conducting material like multiwalled carbon nanotubes (MWCNTs). In an earlier report, a hydrothermally synthesized TiO_2-MWCNTs based DSSC delivered a PCE of 7.37%, compared to a PCE of only 4.9% obtained for its' TiO_2 based analogue, thus illustrating that MWCNTs facilitate fast electron transport to the external circuit and improve efficiencies. [6] Among QDs, a narrow gap QD such as PbS or PbSe with a band gap in the near infrared (NIR) region [6-10] is preferred over visible light absorbing QDs such as CdSe or CdS, [11-17] for broader spectral utilization is possible with the NIR absorbing QDs, thus manifesting in increased charge separation and collection. For a ZnO/PbS QDs/graphene based solar cell, a PCE of ~6.36% was achieved compared to ~5.28% for an equivalent cell without graphene. Authors propounded that conductive graphene helps in extracting charges. [18] Ozone treated PbS QDs based organic solar cell gave an efficiency of 1.68%, which was higher than that delivered by air-annealed devices. [19] Low

[a] Department of Chemistry, Indian Institute of Technology Hyderabad, kandi-502285, Sangareddy, Telangana India
[b] Department of Biomedical Engineering, Department of Mechanical Engineering, University of Bridgeport, Bridgeport, CT 06604
[c] Department of Mechanical Engineering, University of Bridgeport, Bridgeport, CT 06604
[d] Biology Department, Wesleyan University, Middletown, CT 06459
† E-mail: mdeepa@iith.ac.in Tel: +91-40-23016024, Fax: +91-40-23016003.
Electronic Supplementary Information (ESI) available: J-V plots of photoanode with spacer and without spacer. Solar cell parameters of QDSCs (with standard deviation). CV plots of photoanode and counter electrode components. CB and VB position calculations. See DOI: 10.1039/x0xx00000x

optical absorption and high series resistance of the air-annealed device were responsible for its poor response. In another recent study, a ZnO/PbS QDs based cell produced a PCE of 6%. [10] In the above-described reports, the external quantum efficiencies (EQEs) span from the visible to the NIR region (> 800 nm), extending even up to 1400 nm, thus implying that PbS QDs are very effective in harvesting longer wavelengths.

Besides customizing the wide gap semiconductor and the photosensitizer, the TiO_2/QDs/electrolyte interface can also be engineered to suppress back electron transfer to the oxidized species in the electrolyte and to the intra-gap states introduced by the defects in QDs, the key reasons for the lower PCEs of QDSCs compared to DSSCs and even organic solar cells. In the recent past, the application of passivating layers of ZnS or SiO_2 or amorphous TiO_2 and their blends over TiO_2/CdSeTe QDs based photoanodes, proved to be extremely successful in reducing electron recombination. [15, 20-22] These layers passivate the surface trap states on QDs, and also of the TiO_2 surfaces uncovered by QDs, thereby decrease charge recombination, and enhance efficiencies. PCEs in the range of 8.2-10% have been achieved by the use such interfacial barrier layers. [15, 20-22] In another study, fumed silica nanoparticles (SiO_2 NPs) were incorporated in a polysulfide electrolyte to regulate the TiO_2/QDs/electrolyte interface of $CdSe_xTe_{1-x}$ QDSCs and authors observed that both fill factor (FF) and open circuit voltage (V_{OC}) increased in the presence of this electrolyte additive. [23] Authors deduced that SiO_2 not only gels the liquid polysulfide electrolyte, but also inhibits interfacial recombination to improve the cell performance, as PCE increased from 8.73% (at 0 wt% SiO_2) to 11.73% (at 3 wt% of SiO_2). [23]

Another factor that controls QDSC performance is the counter electrode (CE). Low cost, high electrocatalytic activity towards sulfide reduction, high electrical conductivity, and a chemically robust structure are the desirable characteristics in a counter electrode. Tin sulfide (SnS) is an attractive option for a CE, for it satisfies these pre-conditions, and while it has been employed in a DSSC previously, [24] it has not been used in a QDSC till date. Efficiency of a SnS nanosheets based DSSC was 6.56%, as opposed to 7.57% obtained for the same cell with a Pt CE. The short circuit current densities of the two cells were found to be comparable (J_{SC} ~ 17.7 and 17.5 mA cm^{-2}), which highlighted the good catalytic activity of the SnS based CE. [24]

In the present report, with the objective of developing high performance QDSCs, the cell architecture is designed by incorporating the following elements. (a) A TiO_2-MWCNTs based composite (instead of TiO_2) is used for anchoring PbS QDs, to enhance the charge collection capability of the photoanode. (b) PbS QDs with a band gap of 1.1 eV are used for wider spectral conversion to electricity. (c) A gel electrolyte dispersed with electrochemically inert TiO_2 NPs is used as the hole transport material, to curb interfacial recombination. (d) A CE, new in QDSCs, namely, SnS Nanoparticles (NPs) tethered to a carbon (C)-fabric is employed. The resulting QDSC configuration of TiO_2-MWCNTs/PbS/ZnS-S^{2-}/PVA/TiO_2-SnS/C-fabric shows excellent solar cell performance, and how each of the aforementioned strategies influence cell performance is studied in detail. The novel cell configuration coupled with the features incorporated in the cell are expected to be of great use in developing cells with robust, stable performances.

Experimental section

Materials

Fluorine doped tin oxide (FTO) glass substrates with a sheet resistance of ~25 Ω cm^{-2} were purchased from Pilkington and were cleaned in a soap solution, 30% HCl solution, twice distilled water and acetone, in that order, before use. Titanium isopropoxide, Ethyl cellulose (EC), terpineol, MWCNTs, 1-octadecene (ODE), 1,2-ethanedithiol (EDT), trioctylphosphine (TOP), thioacetamide, bis[bis(trimethylsilyl)amino]tin(II), ([Sn-[$N(SiMe_3)_2]_2$], poly(vinyl alcohol) (PVA) and sodium sulfide (Na_2S) were purchased from Aldrich. Oleic acid, acetonitrile, hexane, acetone, 3-mercaptopropionic acid, sulfuric acid (H_2SO_4) and nitric acid were purchased from Merck. Bis(trimethylsilyl)sulfide (TMS) was purchased from TCI. Ultra-pure water with a resistivity of ~18.2 MΩ cm was obtained through a Millipore Direct-Q 3 UV system. TiO_2-P25 nanoparticles were a free gift from Evonik.

Preparation of photoanode

Preparation of TiO_2-MWCNTs*:*

The TiO_2-MWCNTs nanocomposites were synthesized using a hydrothermal method previously reported by Muduli et al. [6] 2 mL of titanium isopropoxide was hydrolyzed with 5 mL of deionized water and 0.5 wt% of acid functionalized MWCNTs [25, 26] were added to this solution, which was followed by sonication for 10 min. The solution was then transferred to a Teflon-lined autoclave along with 5% H_2SO_4 solution. The autoclave vessel was maintained at 175 °C temperature for 24 h. The obtained product was filtered and washed with deionized water 3-4 times and then dried in a hot air oven at 60 °C for over a day. Pristine TiO_2 was also prepared by using the same procedure without the addition of MWCNTs.

Preparation of PbS QDs:

PbS QDs were synthesized by using a method proposed by Ushakova et al. [27] PbO (1 mmol) was dissolved in oleic acid (4 mmol) and 10 mL of 1-octadecene in a three necked 25 mL flask and degassed with argon flow for 30 min. with constant stirring and the reaction mixture was heated to 170 °C for 1 h until it formed a clear solution which indicated the formation of lead oleate precursor solution. Next, the sulfur precursor containing 0.2 mmol of TMS in 0.5 mL of 1-octadecene was injected into the above solution at 120 °C, and then the resulting solution was kept at this temperature for 15 min. to yield a dark-brown colored solution of PbS QDs. PbS QDs were purified and precipitated with ethanol and hexane for 4-5 times. PbS QDs were dispersed in chloroform for all preparations and characterizations.

Synthesis of SnS NPs:

SnS NPs were prepared by using a procedure reported by Hickey et al. [28] 0.78 mL (2 mmol) of bis[bis(trimethylsilyl)amino]tin(II), 5 mL (15.6 mmol) of 1-octadecene, 3 mL (6.7 mmol) of trioctylphosphine and 4.5 mL (14.2 mmol) of oleic acid were taken in a three necked round bottom flask and degassed under the argon for 30 min. with constant stirring and the reaction mixture was maintained at 170 °C for 30 min to form a clear solution. A solution containing 10 mL (30.4 mmol) of oleylamine, 3 ml (6.7 mmol) of TOP and 0.075g (1 mmol) of thioacetamide was quickly injected into the above solution at 150 °C, and the solution was held at this temperature for 5 min. By the addition of this solution, the color changed from colorless to red and then to dark brown. The solution was cooled to room temperature and was purified and precipitated with ethanol and dispersed in chloroform for further use.

2.2.4 Preparation of TiO_2-MWCNTs paste*:*

A paste of TiO_2-MWCNTs was prepared by a protocol used by Du et al. [29] 2.0 g of TiO_2-MWCNTs were mixed with 15.2 mL of ethanol in a round bottom flask and this dispersion was sonicated for 10 min. Then, 8.1 g of terpineol and 10.4 g of ethanol solution with 10 wt% EC were dispersed in the same and sonicated for 10 min. Ethanol was evaporated through rotary evaporator and a TiO_2-MWCNTs paste was obtained. A paste of TiO_2 was also prepared using the same procedure.

Fabrication of photoanode:

For the active layer of TiO_2-MWCNTs, the above prepared paste was deposited on a FTO substrate by a doctor blading method and the films were annealed at 80 °C for 30 min., followed by annealing at 500 °C for 30 min. One more layer of TiO_2-MWCNTs was prepared using the same method by applying TiO_2-MWCNTs paste and sequential annealing at 80 and 500 °C for 30 min., at each temperature. The FTO/TiO_2-MWCNTs substrates were dipped in an aqueous solution of 0.4 M $TiCl_4$ at 70 °C for 20 min., and the coated substrates were rinsed in ultrapure water to remove the unabsorbed excess TiO_2 and annealed at 500 °C (temperature increase, at the rate of 5 °C min^{-1}).

Preparation of TiO_2-MWCNTs/QDs electrode:

The TiO_2-MWCNTs coated FTO substrate was immersed in a solution of bifunctional linker molecules (10 wt% 3-mercaptopropionic acid or MPA) in acetonitrile for 12 h. Chemical bath deposition (CBD) method was used for the deposition of PbS QDs. Linker coated FTO/TiO_2-MWCNTs films were kept submerged in a PbS QDs solution in chloroform with concentration of 30 mg mL^{-1} for 4 h at room temperature. The films were rinsed in chloroform and stored in dark at 45 °C.

Fabrication of CEs and QDSCs:

SnS/C-fabric electrodes were prepared by drop casting of SnS NPs over C-fabric. Cell fabrication was accomplished in a sandwich manner. Two layers of ZnS were deposited over the photoanode by SILAR, using 0.1 M $Zn(OAc)_2$ and 0.1 M Na_2S baths. A 120 μm thick double-sided tape was used as a spacer between the photoanode and the CE (SnS/C-fabric or C-fabric). The double-sided tape was affixed along the periphery of the photoanode area. 10 wt% of poly(vinyl alcohol) was dissolved in deionized water and heated to a temperature of 90 °C for 2 h to form a gel, then cooled to room temperature. 0.1 M Na_2S, and 0.1 M KCl were dissolved in the above gel, and 0.1 mmol of TiO_2 P-25 NPs were dispersed in the above gel. The cavity was filled with the gel. For supporting the CE, the SnS/C-fabric or C-fabric electrode was glued to a glass slide, and it was placed over the photoanode/spacer assembly with the SnS side facing the photoanode. The whole assembly was held together with binder clips, and the cells were exposed to light from the rear side for all measurements. A cartoon illustrating the preparation of the photoanode and QDSC is shown in Scheme 1.

Characterization techniques

Optical absorption spectra were measured on a UV-Vis-NIR spectrophotometer (Shimadzu UV-3600) for a dispersion of PbS QDs in chloroform in a quartz cuvette in absorbance mode and for films of TiO_2, TiO_2-MWCNTs and TiO_2-MWCNTs/PbS coated on micro-slide glass plates in diffuse reflectance mode, and converted to absorbance using a Kubelka-Munk function. X-ray diffraction (XRD) patterns of samples were recorded on a PANalytical, X'PertPRO instrument with Cu-Kα (λ = 1.5406 Å) radiation. Raman spectra of TiO_2 and TiO_2-MWCNTs were recorded on a Bruker Senterra Dispersive Raman Microscope spectrometer; the laser excitation wavelength was fixed at 532 nm. Surface morphology analysis of electrodes was performed using a scanning electron microscope (ZEISS EVO 18 Special Edition). Transmission electron microscopy studies were carried out on a JEOL JEM-1011 and JEOL 3010 (with an accelerating voltage of 200 kV) microscopes. Samples were extracted into a volatile solvent, and then applied to grids, and measurements were performed after solvent evaporation.

A LOT-Oriel solar simulator equipped with a 150 W Xe lamp, an AM 1.5 filter, capable of delivering an collimated output beam of 25 mm diameter, was coupled with a Metrohm Autolab PSTAT302N and was used for measuring the current *versus* potential (I-V) data of QDSCs, under 1 sun (100 mW cm^{-2}) illumination. The spatial uniformity of irradiance was confirmed by calibrating with a 2 cm × 2 cm Si reference cell and re-affirmed with an ILT1400 radiometer/photometer. External quantum efficiency (EQE) plots were recorded using a Quantum Efficiency Measurement System, Oriel IQE-200™ capable of measurements compliant to ASTM E1021-06. The light source was a 250 W quartz tungsten halogen lamp; the monochromator path length was 1/8M spot and the size was 1 mm × 2.5 mm rectangular at focus. Cyclic voltammograms of pristine- TiO_2, PbS and SnS films deposited over FTO substrates, SnS coated C-fabric were recorded in a three electrode cell, with the aforementioned as working electrodes, a Pt rod as the counter electrode and an Ag/AgCl/KCl as the reference electrode in an aqueous 0.1 M KCl electrolyte solution with a PSTAT302N with a NOVA 1.11.2 software. Linear sweep voltammograms (LSVs) of SnS/C-fabric and C-fabric were recorded by a two probe method by using two needle like

stainless steel probes set apart by 1 cm, at a scan rate of 10 mV s^{-1}. Conductive atomic force microscopy (C-AFM) measurements of TiO_2 and TiO_2-MWCNTs deposited over FTO/glass substrates were carried out on a Veeco Nanoscope (with multimode scan) atomic force microscope. For C-AFM, cantilevers made of antimony doped silicon (n-doped; resistivity ~0.01 - 0.025 Ω cm) and coated with Pt/Ir (20 nm) on the front and backside are used. The spring constant of the tip is 0.2 N/m. The current sensitivity is 1 nA/V and a load force of 47.6 nN is maintained between the tip and the sample. The sample deposited on FTO coated glass, (area ~9 mm^2) is attached to a stainless steel support with a conducting carbon tape. A pin-hole free silver paste coating is applied from the surface of the active film, along the edge of the conducting glass substrate to the stainless steel support, and the topography and current images are recorded at room temperature. The contact tip is scanned in contact with the sample surface. The z-feedback loop uses the dc cantilever defending a signal to maintain a constant force between the tip and the sample to generate topography images. Concurrently, a dc bias of 50 mV is applied to the tip. The sample is held at ground potential. The built-in pre-amplified scanner head measured the current passing through the tip and sample and imaged the current profiles.

Results and discussion

Light absorption and conversion studies

The absorption spectra of different photosensitizers: TiO_2, TiO_2-MWCNTs, PbS and TiO_2-MWCNTs/PbS are shown in the Figure 1a. Pristine TiO_2 film shows a broad absorption below 400 nm and from the absorption edge by using the relation: E_g (eV) = 1240/λ (nm), the band gap of TiO_2 was deduced to be 3.11 eV. The absorption band of TiO_2-MWCNTs composite is broader and the absorption edge is slightly red-shifted, compared to TiO_2. The band gap is 3.07 eV. PbS QDs show a broad absorption band in the 400 to 640 nm wavelength span in the visible region, and an additional broad peak with a λ_{max} at 1130 nm is observed in the near infrared (NIR) region. The band gap is calculated to be 1.1 eV. The TiO_2-MWCNTs/PbS photoanode absorbs in the visible and in the NIR region, as the spectrum of this assembly shows a broad band in the visible region and a peak at 1130 nm. The cumulative effects of TiO_2-MWCNTs and PbS are observed in the absorbance features of this photoanode.

QDSCs are constructed with the following photoanodes: TiO_2/PbS/ZnS and TiO_2-MWCNTs/PbS/ZnS electrodes. C-fabric and SnS coated C-fabric are used as CEs and a gel containing poly(vinyl alcohol), KCl , TiO_2 NPs and 0.1 M Na_2S serves as the hole transport material. Here, KCl acts as a supporting electrolyte, PVA acts as a gelatinizing agent and TiO_2 is used as a filler and as a passivating additive. When the TiO_2 NPs come in contact with the photoanode assembly, they can serve as a supplementary blocking layer, in addition to the ZnS layers coated over the QDs, and like ZnS, prevent electron trapping in the intra-gap states in the QDs, and restrict recombination with the oxidized S_n^{2-} species in the electrolyte. J-V characteristics were recorded for the cells, under an irradiance of 100 mW cm^{-2} (AM 1.5 spectrum) and the respective plots are shown in the Figure 1b and the parameters are summarized in the Table 1, and the average values are listed in Table S1 (supporting information). For the cell based on TiO_2/PbS/ZnS with a C-fabric as CE, the PCE of the champion cell is 3.75% with an open circuit voltage, V_{OC} = 831 mV, J_{SC} = 16.07 mA cm^{-2} and having the highest fill factor (FF = 39%), among all the cells used in this report. The cell with the same photoanode, TiO_2/PbS/ZnS and with SnS coated C-fabric as CE, achieves an efficiency of 4.45%, with a V_{OC} = 880.13 mV, J_{SC} = 16.07 mA cm^{-2} and FF = 36.6%. PCE increases by 18% with SnS/C-fabric based cell relative to the C-fabric based one. The superior electrocatalytic activity and greater electrical conductivity of SnS/C-fabric over C-fabric allows fast electron transfer from the external circuit to the redox couple, thus resulting in better charge separation and higher V_{OC}. The cell with TiO_2-MWCNTs/PbS/ZnS as photoanode and C-fabric as CE, the PCE of the champion cell is 5.41%, with V_{OC} = 834 mV, J_{SC} = 18.3 mA cm^{-2} and FF = 35.4%. PCE of this cell is increased by 44% when compared to the equivalent cell with a TiO_2/PbS film as the photoanode.

The role of MWCNTs as efficient electron conduits, which extract the photoexcited charges from the conduction bands (CBs) of TiO_2 and PbS QDs, and deliver them to FTO, is evidenced by comparing the two cell (with and without MWCNTs) responses. The energy band diagram in Figure 1c shows that the Fermi level of MWCNTs is favorably poised at 4.5 eV, below the CBs of TiO_2 and PbS QDs at 4.2 and 4.08 eV respectively, and above the work function of FTO (~4.7 eV). Photoexcited electrons in PbS QDs can depopulate by cascading to the CB of TiO_2 (then to the Fermi level (E_F) of MWCNTs and then to FTO) or can directly relay to the E_F of MWCNTs. The positions of CBs and valence bands (VBs) are determined by combining the data obtained from cyclic voltammetric studies (Figure S1, supporting information) and optical band gaps. The role of CE in controlling the cell performance, is judged by comparing the two cells with TiO_2-MWCNTs/PbS/ZnS as photoanode, but with SnS/C-fabric and C-fabric as CEs. The cell with a SnS/C-fabric CE delivers the highest PCE among all cells studied here, and the champion cell's PCE is 6.3%, with the highest V_{OC} = 900 mV, J_{SC} = 20 mA cm^{-2} and a FF = 35%. This cell's counterpart with a C-fabric CE, gives a PCE of 5.41%. Further, the Fermi level or valence band maximum of SnS NPs is positioned at ~5.1 eV (Figure 1c). Electrons from the external circuit are injected to the E_F of SnS via the conductive C-fabric, and they readily reduce S_n^{2-} species, which leads to the enhanced performance. Representative dark current profile of the cell with the TiO_2-MWCNTs/PbS-gel-SnS/C-fabric configuration (Figure 1a), shows that the dark current density varies from 0.09 to 0.24 mA cm^{-2}. Previously, dark current densities in the range of -2 to +2 mA cm^{-2} have been observed over a potential range of -0.4 to +0.6 V for PbS based QDSCs. [30] TiO_2 NPs in the electrolyte also help in improving cell performance. A comparison of J-V characteristics of similar cells, with and without TiO_2 NPs in the electrolyte, is shown in Figure S2 (supporting information). With TiO_2 NPs, the efficiency of the QDSC is 6.3%, and without the filler, this efficiency is 6%. The NPs modify the surface of the

TiO_2-MWCNTs/PbS film, induce a passivating effect, which prevents trapping of electrons in the defect states of PbS QDs.

The ability of MWCNTs to promote charge extraction was gauged from fluorescence quenching studies. Fluorescence spectra of PbS QDs, TiO_2/PbS and TiO_2-MWCNTs/PbS films obtained at an excitation wavelength of 379 nm are shown in Figure 2a. PbS QDs show a broad emission in the visible region, with three λ_{max} values at 408, 434, and 459 nm. This emission in all likelihood, stems from the deactivation of electrons which are excited from the levels below the valence band maximum to the levels above the conduction band maximum, i.e., corresponding to energies in excess of the band gap. The visible light excitation is depicted in Figure 1c. The intensity of this emission is quenched in the presence of TiO_2 (in TiO_2/PbS), and further quenched in the presence of TiO_2-MWCNTs (in TiO_2-MWCNTs/PbS). The increased florescence quenching observed with MWCNTs, again indicates that MWCNTs facilitate photo-excited charge extraction from PbS.

Plots showing the variation in EQE as a function of wavelength for cells with the two photoanodes: TiO_2/PbS/ZnS and TiO_2-MWCNTs/PbS/ZnS and having the same CE: SnS/C-fabric are presented (Figure 2b). EQE is a ratio of the number of photogenerated electrons to the number of impinging incident photons of a given wavelength. For the TiO_2/PbS/ZnS cell, the maximum EQE is about 40% in the wavelength range of 390 to 500 nm, and EQE has significant values in the UV range (of 340 to 390 nm) and in the red region (500 to 610 nm) and it varies between 2-12% in the wavelength range of 610-650 nm, which coincides with the light absorption regime of PbS. For the TiO_2-MWCNTs/PbS/ZnS cell, the maximum EQE is about 53% in the wavelength range of 370 to 520 nm, and EQE has reasonably good values in the 330 to 370 nm and 520 to 620 nm wavelength range. Thereafter, it lies between 3-15% in the wavelength range of 620-650 nm. MWCNTs are effective in channeling the excited electrons to the external circuit, and this is reflected in the enhanced EQE obtained for the MWCNTs based cell over the entire wavelength range under consideration.

Nanoscale current flow comparison

To understand the role of MWCNTs in promoting charge extraction and transport to FTO in the cells with TiO_2-MWCNTs composite in the photoanode, nanoscale current maps of TiO_2 and TiO_2-MWCNTs are compared. Figure 3 shows the simultaneous topography and current images recorded for films of TiO_2 and TiO_2-MWCNTs on FTO substrates; the scanned area is 700 nm × 700 nm for each film.

The topography of TiO_2 (Figure 3a), shows the presence of aggregated TiO_2 NPs and the dimensions of these agglomerates vary from 20 to 190 nm. The corresponding current image (Figure 3a'), shows a uniform distribution of bright domains over the entire region under consideration. The bright portions are assigned as regions of high current, and the dark regions arise from the low current domains. The average current flowing across the film is ~20 pA, and the maximum current is 90 pA. The reasonable magnitude of current attained in pristine TiO_2 is attributed to charge propagation facilitated by the surface defects such as dangling bonds and oxygen vacancies. The current is color-scaled at the right sides of the current maps. For the TiO_2/MWCNTs electrode, the topography image (Figure 3b) shows uniformly distributed elongated particles, indicating the presence of MWCNTs. In the corresponding current image (Figure 3b'), the bright regions are more closely spaced compared to the current image of TiO_2. The average current flowing across the composite film is ~2 nA, which is almost four orders of magnitude greater than the current carrying capability of pristine TiO_2, and the maximum current is two orders of magnitude higher than that of sole TiO_2, thus confirming that charge transport across the photoanode can be improved by the incorporation of MWCNTs in the assembly. These bright regions can be treated as the localized conducting domains, and their ability conduct electrons is superior to the similar domains in pristine TiO_2, owing to the presence of MWCNTs. The almost seamless distribution of the bright regions indicates that unhindered charge movement is realized in the TiO_2-MWCNTs composite film.

Morphologies and structures

The morphologies of the photoanode films and the CE are shown in Figure 4. The SEM images of pristine TiO_2 (Figure 4a and b) reveal an interconnected network of TiO_2 nanoparticles with no distinct grain boundaries. The films are highly porous with a wide variation in pore dimensions, ranging from 20 to 100 nm. A high loading of QDs across the cross-section of the oxide is possible due to the porous structure. The images of the TiO_2-MWCNTs composite (Figure 4c and d) show particulate morphology, indicating a homogeneous mixing of MWCNTs and TiO_2 NPs. This textured morphology is also very conducive for a good absorption of PbS QDs. The images of TiO_2-MWCNT/PbS film (Figure 4e and f) show intertwined wavy structures which are uniformly distributed over multiple micron length scales. The SEM images of C-fabric (Figure 4g), show that the fabric is composed of solid cylindrical carbon fibers with smooth contours, approximately 5 μm thick, and these interweave and endow the fabric with a mat like appearance, as can be gauged from the photograph in Scheme 1. Upon drop-casting of SnS NPs onto the C-fabric, a SnS/C-fabric CE is obtained, and the corresponding SEM image (Figure 4h) shows that the QDs coat the carbon fibers of the fabric homogeneously and no uncovered portions are visible, implying an intimate contact between the fibers and the QDs, that is most advantageous for fast electron injection from the C-fabric to the Fermi level of SnS NPs during QDSC operation.

The X-ray diffractograms of pristine- TiO_2, TiO_2-MWCNTs, PbS and SnS are shown in Figure 5(a-d). The XRD pattern of pristine TiO_2 shows peaks at d = 3.51, 2.42, 2.37, 1.88, 1.69, 1.66, 1.48, 1.26 Å which correspond to the (101), (103), (004), (200), (105), (211), (204) and (215) planes of the tetragonal body centered cubic lattice, in agreement with powder diffraction file (PDF) # 89-4921. For PbS, the pattern is characterized by distinct peaks at 2θ = 26.09°, 30.10°, 43.07°, 51.00°, 53.41° and 71.01°, corresponding to inter-planar spacings (d) of 3.42, 2.96, 2.09, 1.79, 1.71 and 1.33 Å, and these values match with the (111),

(200), (220), (311), (222) and (420) planes of a face centered cubic lattice of PbS (PDF # 77-0244), thus ratifying the formation of PbS QDs. The diffractogram of SnS NPs shows peaks at 2θ = 26.60°, 31.34°, 31.68°, 38.74°, 50.55° and 52.83° and these correspond to inter-planar distances of 3.35, 2.85, 2.82, 2.31, 1.80 and 1.73 Å, and are assigned to the (021), (100), (130), (131), (151) and (061) planes of the orthorhmbic symmetry of the end centered lattice of SnS (PDF # 32-1361).

Raman spectra of the acid functionalized MWCNTs, TiO_2 and TiO_2-MWCNTs are shown in the Figure 5(a'-c'). MWCNTs show two sets of D and G bands. The fundamental or first order vibrational modes due to the defects (or stretching mode of disordered graphitic carbons) and the in-plane stretching mode of sp^2 hybridized (graphitic) C-C bonds lead to the D and G bands at 1343 and 1577 cm^{-1}, with an I_D/I_G ratio of 1.49. The first overtones, namely, 2D and 2G bands appear at 2677 and 2927 cm^{-1}. Raman (shift) peaks of TiO_2 are observed at 396, 512 and 640 cm^{-1}, characteristic of Ti-O bond vibrations. [6] In the TiO_2-MWCNTs composite, the D and G bands and the 2D and 2G bands (that stem from MWCNTs) show blue-shifts (to higher energies) relative to pristine MWCNTs, whereas the Ti-O modes are slightly red-shifted, compared to TiO_2. These positional shifts, and the line broadening observed in the composite are attributed to the van der Waal's attractive forces between TiO_2 and MWCNTs and the electrostatic interactions between the COO^- groups on MWCNTs and the Ti^{4+} species. In the composite, the I_D/I_G ratio is 0.94. The decrease in this ratio indicates that TiO_2 passivates the surface defects on MWCNTs to some extent.

TEM images of the photo-/electro- active materials are displayed in Figure 6. The TEM image of mono-disperse PbS QDs and the corresponding lattice scale image of PbS QDs are shown in Figure 6a and b. The images show discrete PbS quantum dots, with sizes in the range of 3 to 8 nm. QDs with inter-fringe separations of 0.34 and 0.17 nm are observed, and these match well with inter-planar spacings of 3.42 and 1.71 Å, corresponding to the (111) and (222) planes of PbS with a fcc lattice. The TEM image of TiO_2 (Figure 6c) shows agglomerated particles of TiO_2, and in some regions, distinct grains of TiO_2 are observed. The NP dimensions vary from 10 to 40 nm, which is typical of mesoporous TiO_2. The TEM images of TiO_2-MWCNTs are displayed in Figure 6d and e. The images show aggregated nanoparticles of TiO_2 which appear to be superimposed over the MWCNTs for fuzzy contours of MWCNTs are visible in the images, thus indicating the formation of a homogeneous composite wherein the TiO_2 nanoparticles are uniformly tethered to the CNTs. The TEM images of TiO_2-MWCNTs/PbS (Figure 6f and g) show PbS QDs and TiO_2 NPs anchored to the elongated structures of MWCNTs. Grains with dimensions below 10 nm are in all likelihood, PbS, and the larger sized grains are TiO_2. TEM images of SnS NPs are presented in Figures 6h and i. The particles have elliptical shapes, and their dimensions are in the range of 5-20 nm.

Charge transfer and transport studies

Electrochemical impedance spectra of QDSCs with TiO_2/PbS/ZnS and TiO_2-MWCNTs/PbS/ZnS as photoanodes, and with SnS/C-fabric as CEs were recorded under 30 mW cm^{-2} white light illumination, at an ac amplitude of 20 mV. The Nyquist and Bode plots recorded under short circuit (V_{dc} = 0 V) and open circuit (V_{dc} = 0.75 V) conditions, and over a frequency range of 1 MHz to 0.1 Hz are shown in Figure 7a and b, and the parameters were tabulated in Table 2. Bulk resistance (R_b) and electron transport resistance (R_e) for the TiO_2-MWCNTs/PbS/ZnS electrode is smaller than that of the TiO_2/PbS/ZnS electrode under short circuit conditions. R_e is the measure of the resistance offered by the TiO_2/PbS or TiO_2-MWCNT/PbS interface for electron transfer. Fast electron transfer from the CB of TiO_2 or from the CB of PbS, to FTO in the TiO_2-MWCNTs composite based cell is enabled by MWCNTs, due to their high electrical conductivity and a suitably positioned Fermi level, and therefore R_e is much lower (45 Ω cm^2) in comparison to the TiO_2 based cell (R_e ~ 96 Ω cm^2). Electron recombination resistance (R_{rec}) at the TiO_2/QDs and electrolyte interface, is obtained open circuit and it is 52 Ω cm^2 for the cell without MWCNTs and 59 Ω cm^2 for the one with the MWCNTs in the photoanode, indicating that recombination, is also to some extent increased by MWCNTs. Chemical capacitance (C_μ) is a measure of the electron density in the CB of TiO_2, and exhibits an exponential increase, when TiO_2 has a good conductivity. [31] C_μ, is also found to be higher for the TiO_2-MWCNTs/PbS/ZnS cells, compared to the TiO_2/PbS/ZnS cells, indicating a higher electron population in the CB of TiO_2 in the presence of MWCNTs, which can also be correlated to the higher J_{SC} obtained for the composite based cell. In the low frequency straight-line region, the parameter, Y_o, represents the ease of diffusion of electrons, under zero dc bias. Y_o is nearly three-fold times greater for the MWCNTs electrode based cell compared to one devoid of MWCNTs.

From the Bode phase plot (Figure 7b), both the electron transit time and electron recombination time for the photoanode can be determined at short-circuit and open circuit conditions. Electron transit time τ_d, is the time taken by the photoexcited electron to reach the current collector through the CB of TiO_2. τ_d can be calculated from the expression $\tau_d = 1/2\pi f$, where f is the frequency of the maximum imaginary component. τ_d for the TiO_2-MWCNTs/PbS/ZnS is 0.04 ns which is faster than that of the TiO_2/PbS/ZnS 0.06 ns. Electron recombination time, τ_n, is the time taken by the photoexcited electron to recombine with the oxidized species of the electrolyte. τ_n for the TiO_2-MWCNTs/PbS/ZnS cell is 0.27 ns, and for the TiO_2/PbS/ZnS cell, it is 0.39 ns. For a good solar cell performance, τ_d should be shorter than τ_n.

To evaluate the charge transfer capability of SnS/C-fabric CE in comparison to C-fabric as a CE, symmetric cells were constructed with the sulfide based gel electrolyte (containing KCl, Na_2S, PVA and TiO_2 NPs) and impedance spectra were recorded (Figure 7c and d) and the fitting parameters are provided in Table 3. In this method, the same material serves as a working electrode and counter electrode. R_b or the bulk resistance offered by the electrolyte is comparable for both cells (~8-10 Ω cm^2). R_{ct}, represents the catalytic activity of the electroactive electrode at the electrode/electrolyte interface, and is obtained from the radius of the first semicircle. R_{ct} for the

symmetric SnS/C-fabric cell is 3.6 Ω cm^2 and for the analogous C-fabric cell, it is 6.3 Ω cm^2. The SnS/C-fabric cell shows lesser resistance to charge transfer than the C-fabric cell. Poor charge transfer rate at the CE, typically results in a high overpotential for S_n^{2-} reduction, which blocks electron flow, and promotes back electron transfer at the photoanode. [32] The lower J_{SC} obtained for cells with C-fabric, compared to the SnS/C-fabric cells reflect the effect of this R_{ct} differential. C_{dl}, represents the double layer capacitance at the electrode/electrolyte interface due to the accumulation of the ions at the electrode surface. Higher the C_{dl} for an electrode, better is the electrocatalytic activity. The SnS/C-fabric cell shows a high C_{dl} of 12.4 μF cm^2 compared with that to 3.5 μF cm^2 (obtained for the C-fabric cell). Here, the Bode plot gives the time for charge diffusion across the cross-section of the electrode. The diffusional time is 0.35 s for the SnS/C-fabric electrode, as opposed to 0.45 s for indicating a faster electron propagation compared to the C-fabric cell.

The electrocatalytic activities of the two electrodes: SnS/C-fabric and C-fabric are compared from their LSV plots (Figure 7e) measured in the gel electrolyte, with Pt as a counter electrode and Ag/AgCl/KCl as the reference electrode, over a potential range of −0.9 to +0.3 V. In the reduction sweep of the voltammograms, broad peaks are observed at −0.57 and −0.46 V for C-fabric and SnS/C-fabric. The peaks are due to the following reduction reaction.

$$S_n^{2-} + 2e^- \rightarrow S_{n-1}^{2-} + S^{2-} \quad (1)$$

The redox potential for this reduction is −0.5 V (versus normal hydrogen electrode (NHE)), [33] which is −0.697 V versus Ag/Ag^+. Here, even with C-fabric, the overpotential (η) for polysulfide species reduction is negative (−0.127 V), indicating that reduction occurs at lower negative potentials than theoretically expected values. It is even more negative with SnS/C-fabric (η = −0.24 V), indicating that SnS NPs catalyse the reduction of polysulfide more efficiently than C-fabric does. Further evidence for the effectiveness of SnS/C-fabric as a CE was obtained by comparing its' I-V profile with that of C-fabric. I-V characteristics of the two electrodes measured over a voltage range of −0.2 to +0.2 V are shown in Figure 7f. The plots show an Ohmic behavior over a narrow voltage range of approximately −0.05 to +0.05 V. The slopes of the straight line fits, in the Ohmic regimes, correspond to the conductances of the CE materials, as per the relation ($I/V = 1/R = G$ (Ω^{-1})). The conductances of SnS/C-fabric and C-fabric are 0.06 and 0.15 Ω^{-1}. Since the conductance of C-fabric is only nominally reduced upon coating with SnS NPs, it is obvious that SnS NPs can easily transmit electrons to oxidized polysulfide species during QDSC operation.

Photovoltage decay

Photovoltage decay is also an important tool to measure charge transfer characteristics and the recombination process of solar cells. [30, 34] The cells were illuminated by a white LED source having a 30 $mWcm^{-2}$ light intensity for 10 s, then a voltage is produced across the cell, and when the light is switched off, charges recombine either with the defect states, or with the electrolyte and the photovoltage decay was monitored as a function of time. Rapid photovoltage decay implies fast recombination, and slower decay infers a greater charge build-up under illumination. [35] Greater the density of electrons accumulated in the QDs or in the CB of TiO_2 upon irradiance, larger is the in-built potential (under illumination off condition), which effectively translates to a higher V_{OC} in a QDSC. The photovoltage decay plots of cells with the two photoanodes: TiO_2/PbS/ZnS and TiO_2-MWCNTs/PbS/ZnS and with the two CEs: C-fabric and SnS/C-fabric are displayed in Figure 8a. MWCNTs in the photoanode, and SnS as the CE enhance photovoltage decay. The decay rate and as a consequence, the recombination rate is lower for the TiO_2-MWCNTs containing photoanode when compared with the only TiO_2 containing cell with the same counter electrode. This is because, recombination is controlled by the density of electrons available for the recombination. Density of electrons available for recombination is less in the case of TiO_2-MWCNTs/PbS than TiO_2/PbS, due to fast electron transfer to FTO. The charge recombination from the CB of TiO_2 or CB of PbS with the intra-gap states in PbS QDs (introduced by the surface defects in QDs) and with the oxidized electrolyte species is diminished with the addition of MWCNTs to TiO_2. It is also observed that the CE also plays a significant role in retarding the decay or recombination process. The cells with SnS/C-fabric CE show slower decay compared to the cells with C-fabric as CE. The higher Voc values obtained with the use of SnS/C-fabric as CE, also indicate that hole extraction from the QD by the electrolyte is faster than back electron transfer to the redox couple.

To affirm the hole conducting capability of the gel electrolyte, Mott-Schottky plots of the gel containing 0.1 M Na_2S, 0.1 M KCl, 0.1 mmol TiO_2 and 10 wt% of PVA in water, were recorded with Pt as working and counter electrodes and an Ag/AgCl/KCl as the reference electrode. Mott-Schottky plots ($1/C^2$ *versus* E) for the gel at two different frequencies of 100 Hz and 1 kHz are shown in the Figure 8b. Negative slopes observed for the plots indicate a p-type semiconducting behavior despite the presence of a n-type semiconducting oxide (TiO_2) in the gel, thus ratifying that the gel works as a hole transport material, which favors the hole scavenging from the VB of PbS to the sulfide redox couple during cell operation.

Conclusions

Three approaches were implemented to improve the performance of a TiO_2/PbS based QDSC. Conventional TiO_2 was replaced by a hydrothermally synthesized TiO_2-MWCNTs composite, a novel counter electrode, SnS NPs tethered to C-fabric was used, and TiO_2 nanoparticles were incorporated as a filler and as a passivating agent in a gel electrolyte. MWCNTs increase the PCE of the QDSC, for they allow rapid charge collection from the CBs of TiO_2 and PbS QDs, due to their high electrical conductivity, and a suitably positioned Fermi level. This was supported by the lower electron transport resistance, and higher recombination resistance obtained for the corresponding cells, and also by their ability to conduct higher

nanoscale currents compared to pristine TiO_2. SnS/C-fabric outperforms plain C-fabric as a CE, for cells with the former show higher efficiencies, and proof for its high catalytic activity for S_n^{2-} reduction was obtained in the form of lower charge transfer resistance, lower reduction potential compared to C-fabric. SnS/C-fabric also contributes towards attaining higher V_{OC} and J_{SC}. This study shows that by careful adjustment of the components of a QDSC, cells with reproducibly good performances can be developed.

Supporting Information

J-V plots of photoanode with spacer and without spacer. Solar cell parameters of QDSCs (with standard deviation). CV plots of photoanode and counter electrode components. CB and VB position calculations This material is available from the Wiley Online Library.

Acknowledgements

Financial support from the Solar Energy Research Initiative-Department of Science & Technology (DST/TM/SERI/2K12-11(G)) is gratefully acknowledged.

Notes and references

1 J. Du, Z. Du, J.S. Hu, Z. Pan, Q. Shen, J. Sun, D. Long, H. Dong, L. Sun, X. Zhong, L. J. Wan, *J. Am. Chem. Soc*., 2016, **138**, 4201-4209.
2 M. Samadpour, P. P. Boix, S. Gimenez, A. I. Zad, N. Taghavinia, I. Mora-Sero, J. Bisquert, *J. Phys. Chem. C,* 2011, **115**, 14400-14407.
3 K. Zhao, Z. Pan, I. M. Sero, E. Canovas, H. Wang, Y. Song, X. Gong, J. Wang, M. Bonn, J. Bisquert, X. Zhong, *J. Am. Chem. Soc*., 2015, **137**, 5602-5609.
4 K. Zhao, Z. Pan, X. Zhong, *J. Phys. Chem. Lett*., 2016, **7**, 406-417.
5 P. Sudhagar, T. Song, D. H. Lee, I. M. Sero, J. Bisquert, M. Laudenslager, W. M. Sigmund, W. I. Park, U. Paik, Y. S. Kang, *J. Phys. Chem. Lett.,* 2011, **2**, 16, 1984-1990.
6 S. Muduli, W. Lee, V. Dhas, S. Mujawar, M. Dubey, K. Vijayamohanan, S. H. Han,S. Ogale, *ACS Appl. Mater*. *Interfaces,* 2009, **1**, 2030-2035.
7 P. N. Kumar, S. Mandal, M. Deepa, A. K. Srivastava, A. G. Joshi, *J. Phys. Chem. C,* 2014, **118**, 18924-18937.
8 Y. Zhang, C. Ding, G. Wu, N. Nakazawa, J. Chang, Y. Ogomi, T. Toyoda, S. Hayase, K. Katayama, Q. Shen, *J. Phys. Chem. C,* 2016, **120**, 28509-28518.
9 B. D. Chernomordik, A. R. Marshall, G. F. Pach, J. M. Luther, M. C. Beard, *Chem. Mater.,* 2017, **29**, 189-198.
10 T. Zhao, E. D. Goodwin, J. Guo, H. Wang, B. T. Diroll, C. B. Murray, C. R. Kagan, *ACS Nano,* 2016, **10**, 9267-9273.
11 R. K. Kokal, P. N. Kumar, M. Deepa, A. K. Srivastava, *J. Mater. Chem. A,* 2015, **3**, 20715-20726.
12 F. Huang, L. Zhang, Q. Zhang, J. Hou, H. Wang, H. Wang, S. Peng, J. Liu, G. Cao, *ACS Appl. Mater. Interfaces,* 2016, **8**, 34482-34489.
13 R. M. Young, S. C. Jensen, K. Edme, Y. Wu, M. D. Krzyaniak, N. A. Vermeulen, E. J. Dale, J. F. Stoddart, E. A. Weiss, M. R. Wasielewski, D. T. Co, *J. Am. Chem. Soc.,* 2016, **138**, 6163-6170.
14 Y. Wu, C. Wadia, W. Ma, B Sadtler, A. P. Alivisatos, *Nano Lett.,* 2008, **8**, 2551-2555.
15 Z. Pan, K. Zhao, J. Wang, H. Zhang, Y. Feng, X. Zhong, *ACS Nano,* 2013, ***7***, 5215-5222.
16 J. Yang, J. Wang, K. Zhao, T. Izuishi Y. Li, Q. Shen, X. Zhong, *J. Phys. Chem. C*, 2015, **119**, 28800-28808.
17 B. Zhang, J. Zheng, X. Li, Y. Fang, L. W. Wang, Y. Lin, F. Pan, *Chem. Commun.,* 2016, **52**, 5706-5709.
18 B. S. Kim, D. C. J. Neo, B. Hou, J. B. Park, Y. Cho, N. Zhang, J. Hong, S. Pak, S. Lee, J. I. Sohn, H. E. Assender, A. A. R. Watt, S. N. Cha, J. M. Kim, *ACS Appl. Mater. Interfaces,* 2016, **8**, 13902-13908.
19 N. Zhao, T. P. Osedach, L. Y. Chang, S. M. Geyer, D. Wanger, M. T. Binda, A. C. Arango, M. G. Bawendi, V. Bulovic, *ACS Nano,* 2010, **4**, 3743-3752.
20 W. Feng, L. Zhao, J. Du, Y. Li, *J. Mater. Chem. A,* 2016, **4**, 14849-14856.
21 H. Zhang, C. Yang, Z. Du, D. Pan, X. Zhong, *J. Mater. Chem. A,* 2017, **5**, 1614-1622.
22 M. T. Nimmo, M. Louis, L. M. Caillard, W. D. Benedetti, H. M. Nguyen, O. Seitz, Y. N. Gartstein, J. Yves,.Y. J. Chabal, A. V. Malko, *ACS Nano,* 2013, **7**, 3236-3245.
23 H. Wei, G. Wang, J. Shi, H. Wu, Y. Luo, D. Li, Q. Meng, *J. Mater. Chem. A,* 2016, **4**, 14194-14203.
24 X. Chen, Y. Hou, B. Zhang, X. H. Yang, H. G. Yang, *Chem. Commun.,* 2013, **49**, 5793-5795.
25 R. Narayanan, M. Deepa, A. K. Srivastava, *J. Mater. Chem. A,* 2013, **1**, 3907-3918.
26 P. N. Kumar, A. Kolay, S. K. Kumar, P. Patra, A. Aphale, A. K. Srivastava, M. Deepa, *ACS Appl. Mater. Interfaces,* 2016, **8**, 27688-27700.
27 E. V. Ushakova, A. P. Litvin, P.S. Parfenov, A. V. Fedorov, M. Artemyev, A. V. Prudnikau, I. D. Rukhlenko, A. V. Baranov, *ACS Nano,* 2012, **6**, 8913-8921.
28 Y. Xu, N. A. Salim, C. W. Bumby, R. D. Tilley, *J. Am. Chem. Soc.,* 2009, **131**, 15990-15991.
29 Z. Du, H. Zhang, H. Bao, X. Zhong, *J. Mater. Chem. A,* 2014, **2**, 13033-13040.
30 B. Ehrler, K. P. Musselman, M. L. Bohm, F. S. F. Morgenstern, Y. Vaynzof, B. Walker, J. L. MacManus-Driscoll, N. C. Greenham, *ACS Nano,* 2013, **7**, 4210-4220.
31 F. F. Santiagoa, J. Bisquert, G. G. Belmonte, G. Boschloo, A. Hagfeldt, Sol. Energ. Mat. Sol. Cells, 2005, **87**, 117-131.
32 I. Hod, A. Zaban, *Langmuir*, 2014, **30**, 7264-7273.
33 V. Jovanovski, V. G. Pedro, S. Gimenez, E. Azaceta, G. Cabanero, H. Grande, R. T. Zaera, I. M. Sero, J. Bisquert, *J. Am. Chem.Soc*., 2011**, 133**, 20156-20159.
34 Z. Pan, X. Zhong, *J. Mater. Chem. A,* 2016, **4**, 18976-18982.
35 M. Shalom, Z. Tachan, Y. Bouhadana, H. N. Barad, A. Zaban, *J. Phys. Chem. Lett.*, 2011, **2**, 1998-2003.

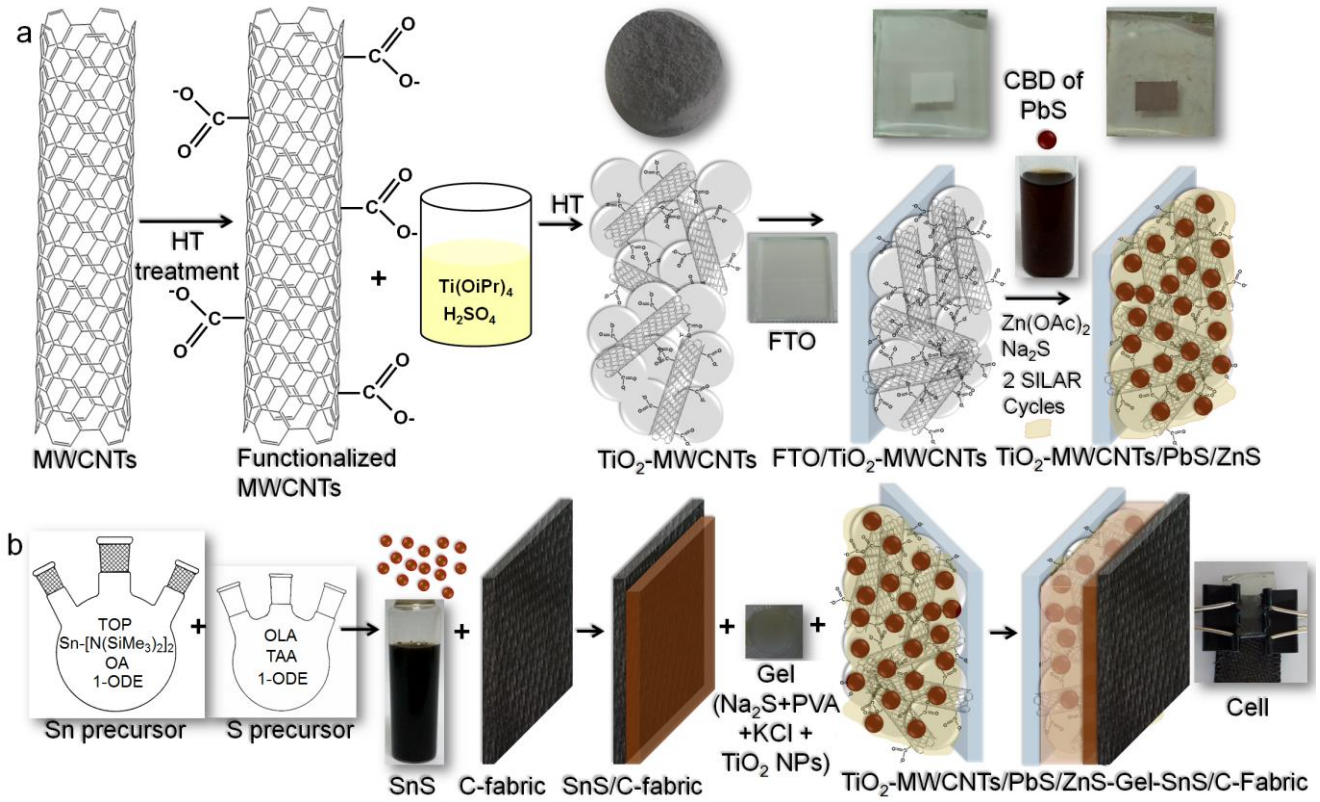

Scheme 1 Cartoon illustrating the preparation of the photoanode, CE and QDSC.

Table 1. Solar cell parameters of QDSCs, exposed cell area: 0.15 to 0.18 cm^2, under 1 sun illumination (100 mW cm^{-2}) with the listed photoanodes and CEs

Photoanode configuration	Counter Electrode	V_{OC} (mV)	J_{SC} (mA cm^{-2})	FF (%)	η_{best} (%)	η_{avg} (%)
TiO_2/PbS	C-fabric	831.3	11.56	39	3.75	3.58±0.17
TiO_2/PbS	SnS/C-fabric	880.1	13.82	36.6	4.45	4.20±0.25
TiO_2-MWCNTs/PbS	C-fabric	833.7	18.31	35.4	5.41	5.28±0.13
TiO_2-MWCNTs/PbS	SnS/C-fabric	900	20.03	35	6.30	6.16±0.14

Table 2 EIS parameters of QDSCs under 30 mWcm-2 white light illumination.

Photoanode	V_{dc} (V)	R_b (Ω cm^2)	R_{rec}/R_e (Ω cm^2)	C_{dl} (μF cm^2)	Y_0 (S $s^{-1/2}$)	τ_n or τ_d (s)
TiO_2/PbS	0.00	53.68	96	5.1	0.93×10^{-3}	0.061
TiO_2-MWCNTs/PbS	0.00	44.1	45	8.2	2.76×10^{-3}	0.042
TiO_2/PbS	0.75	49.23	52	5.7	---	0.39
TiO_2-MWCNTs/PbS	0.75	41.8	59	6.4	---	0.272

Table 3 Fitting parameters for EIS spectra of symmetric cells of CEs: C fabric and SnS/C-fabric under zero dc bias.

CE	R_b (Ω cm^2)	R_{ct} (Ω cm^2)	C_{dl} (μFcm^2)	D (cm^2 s^{-1})	Y_0 (S $s^{-1/2}$)	τ (s)
C-fabric	10.13	6.3	3.5	0.04×10^{-9}	3.7×10^{-2}	0.45
SnS/C-fabric	8.81	3.6	12.4	2.7×10^{-9}	1.4×10^{-2}	0.39

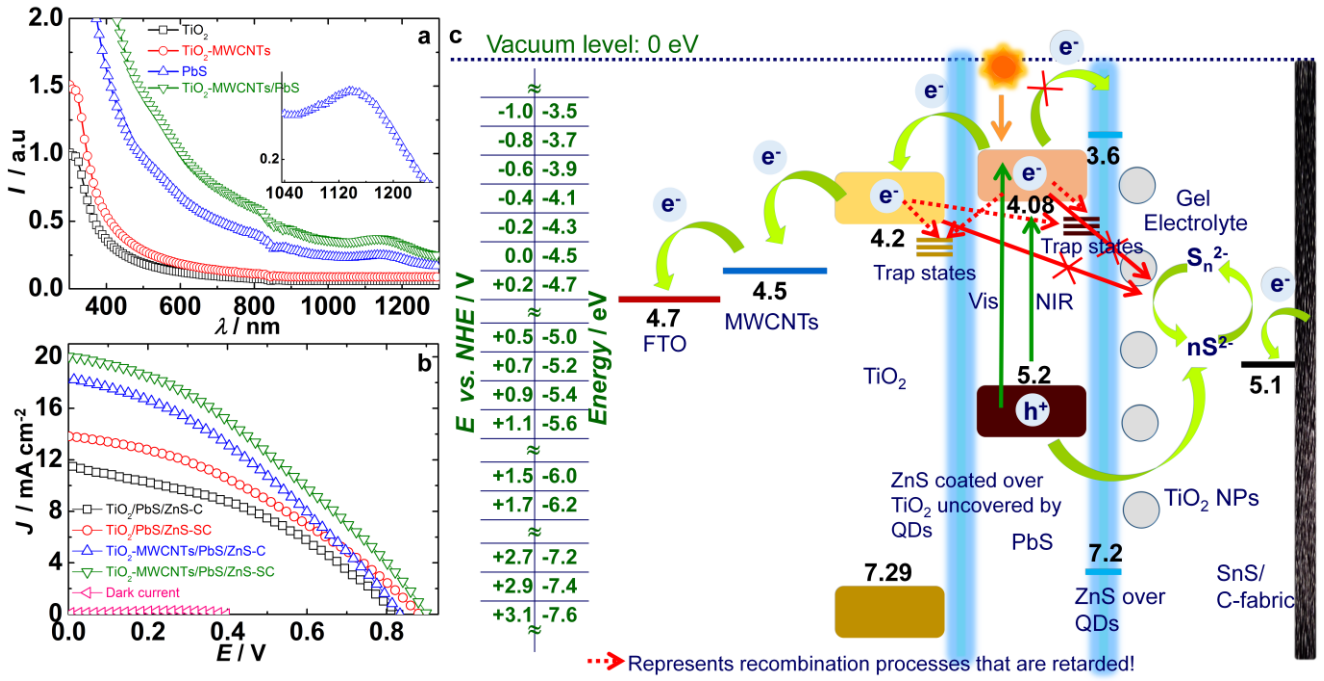

Figure 1 (a) Absorption spectra of pristine TiO_2, TiO_2-MWCNTs, TiO_2/PbS and TiO_2-MWCNTs/PbS films. (b) J-V characteristics of QDSCs with the following photoanodes//counter electrode architectures: TiO_2/PbS/ZnS//C-fabric, TiO_2/PbS/ZnS//SnS/C-fabric, TiO_2-MWCNTs/PbS/ZnS//C-fabric and TiO_2-MWCNTs/PbS/ZnS//SnS/C-fabric. A water based gel containing 10 wt% PVA, 0.1 M KCl, 0.1 mmol of TiO_2 NPs and 0.1 M Na_2S was used as the electrolyte. (c) Energy band diagram of the TiO_2-MWCNTs/PbS/ZnS-gel-CE cell showing all possible electron transfer modes upon illumination.

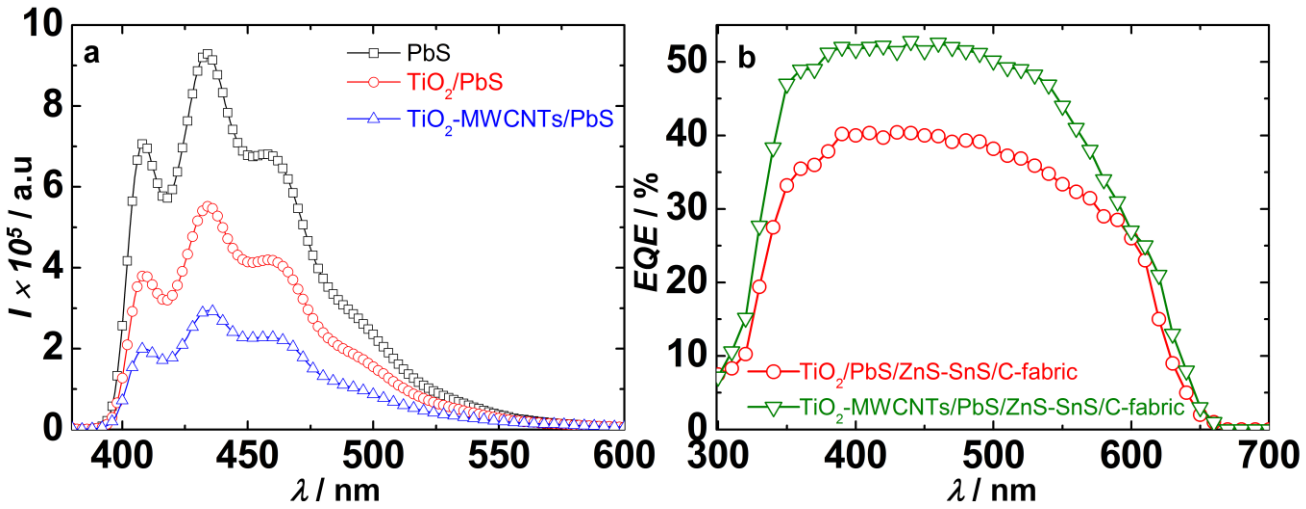

Figure 2 (a) Fluorescence spectra of photoactive films. (b) EQE spectra of QDSCs encompassing the following photoanodes: TiO_2/PbS/ZnS and TiO_2-MWCNTs/PbS/ZnS and with SnS/C-fabric as a CE. A water based gel containing 10 wt% PVA, 0.1 M KCl, 0.1 mmol of TiO_2 NPs and 0.1 M Na_2S was used as the electrolyte.

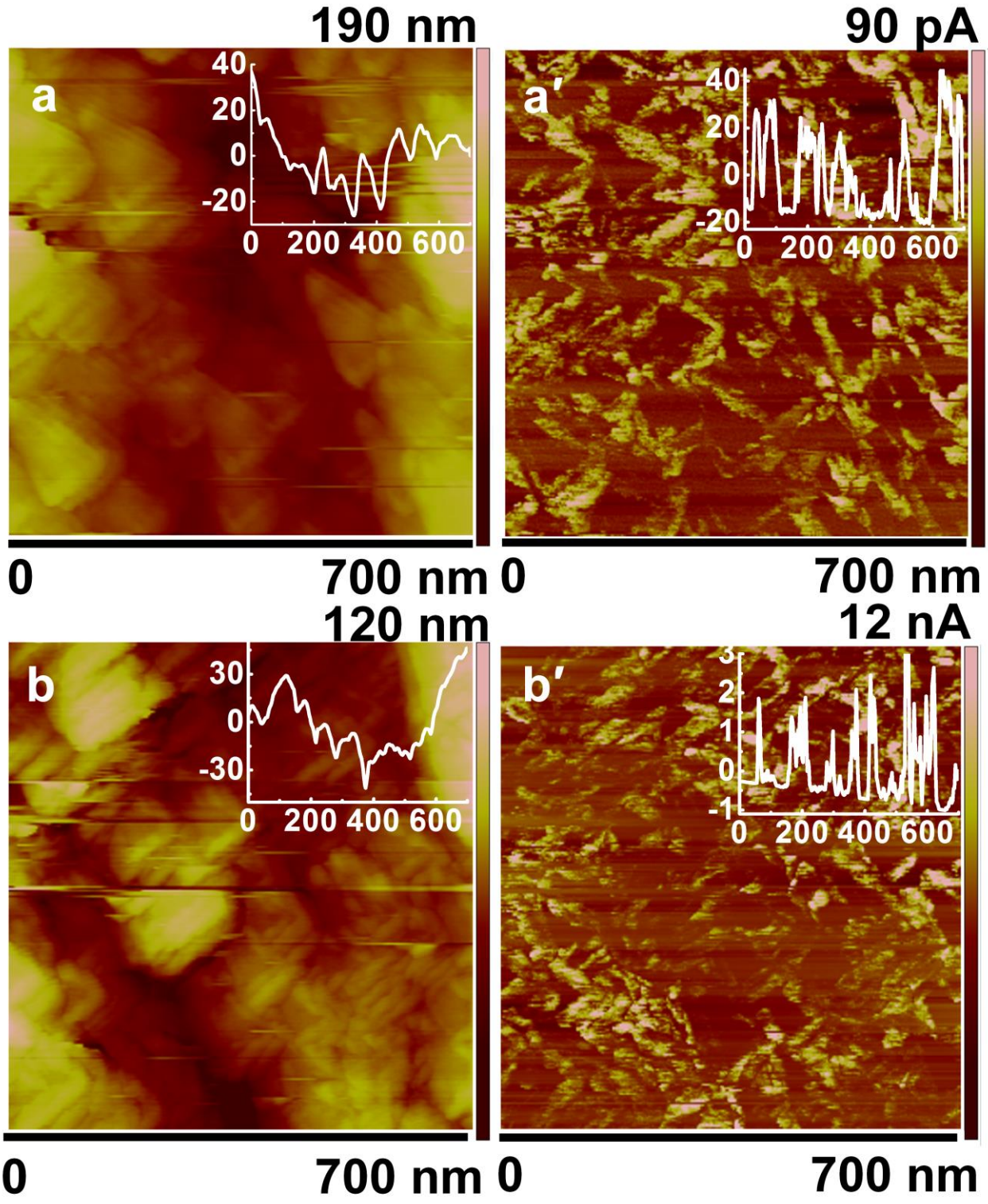

Figure 3 Concurrent topography and C-AFM current images of (a,a′) pristine TiO_2 and (b,b′) TiO_2-MWCNTs. The corresponding section profiles taken along a central line in the images are shown as insets.

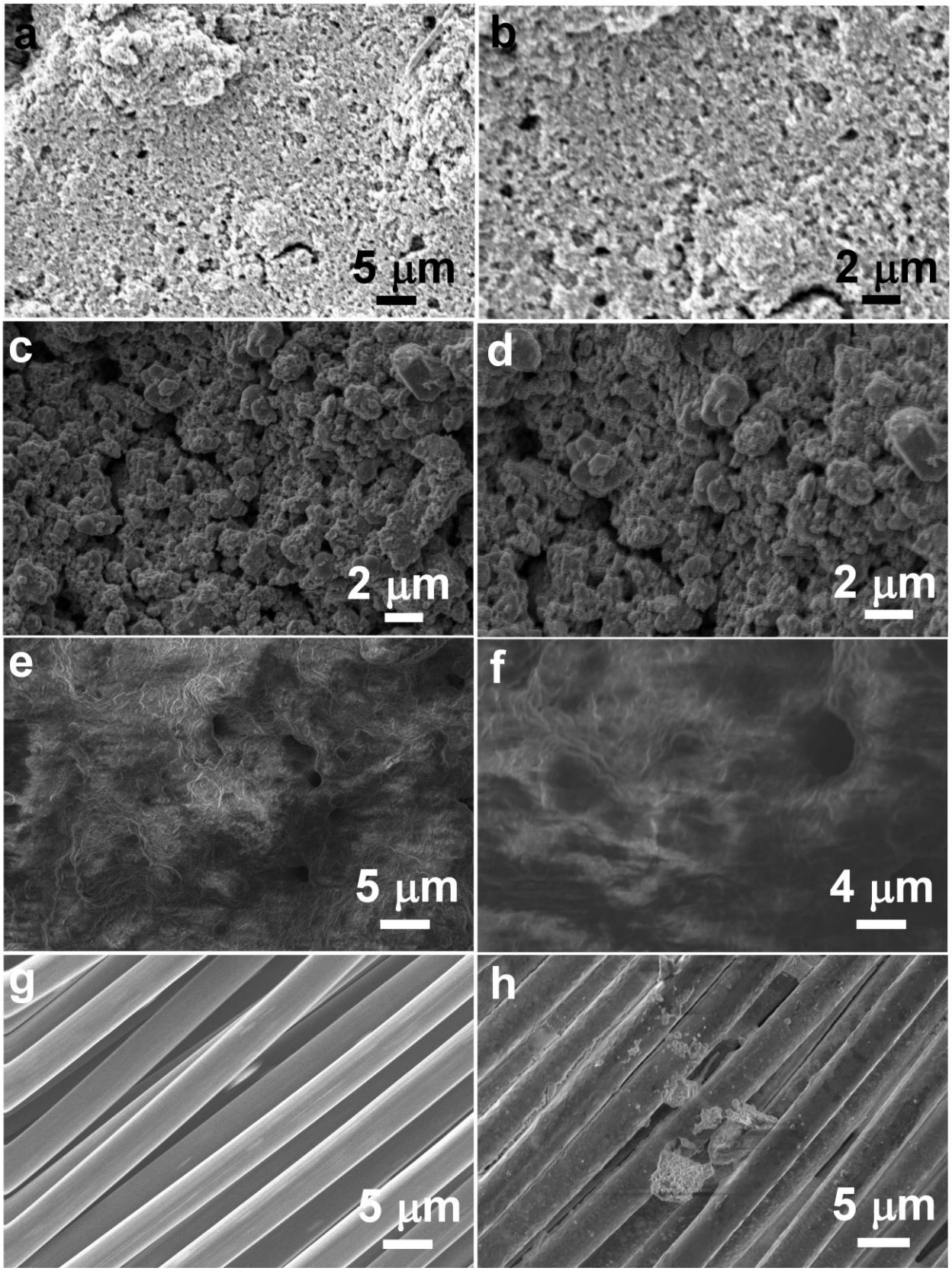

Figure 4 SEM images of (a, b) a pristine TiO_2 electrode, (c, d) a TiO_2-MWCNTs electrode, (e, f) a TiO_2-MWCNTs/PbS electrode, (g) a C-fabric and (h) SnS coated C-fabric at different magnifications.

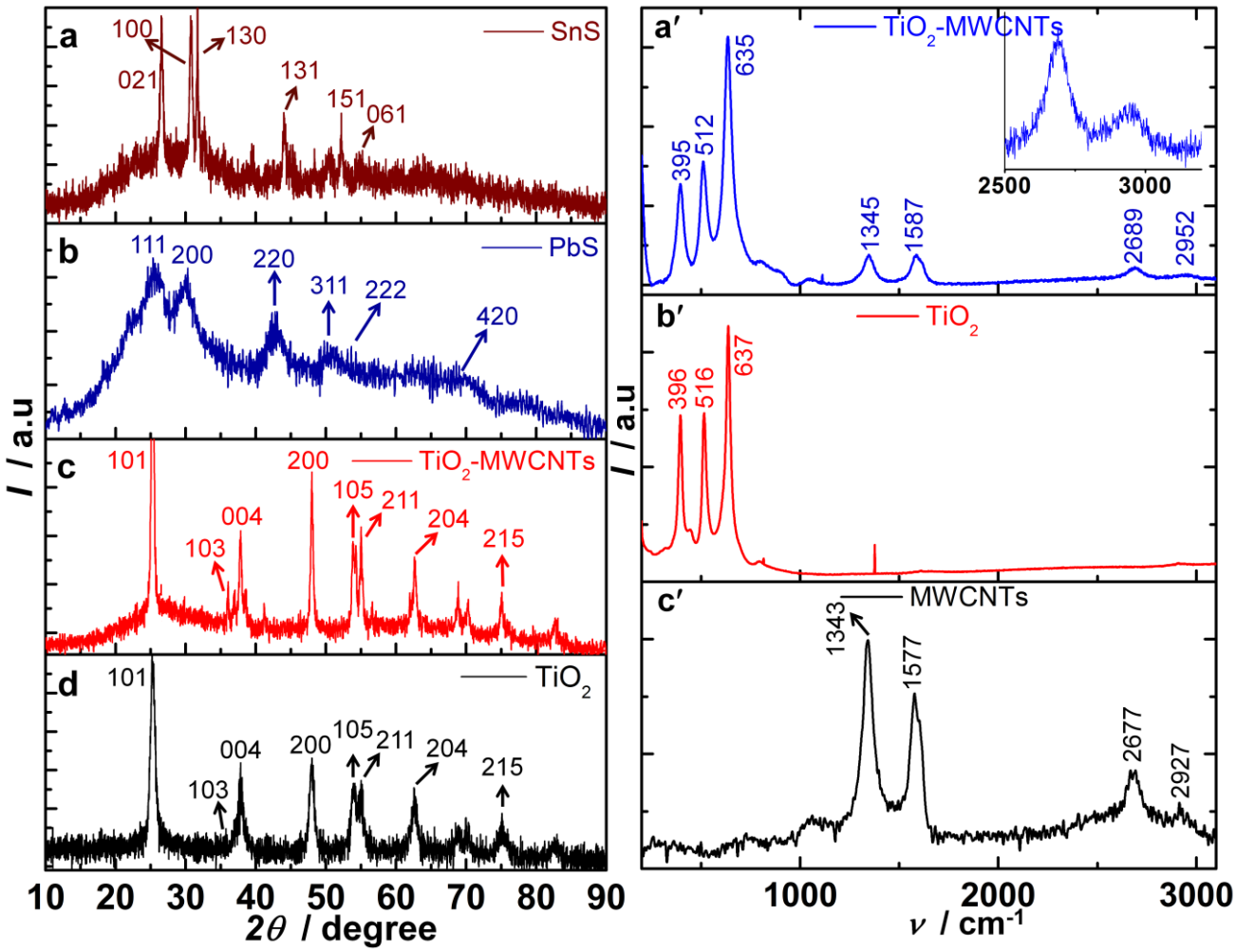

Figure 5 XRD patterns of (a) SnS NPs, (b) PbS QDs, (c) TiO_2-MWCNTs and (d) TiO_2. Raman spectra of (a′) TiO_2-MWCNTs, (b′) TiO_2 and (c′) MWCNTs.

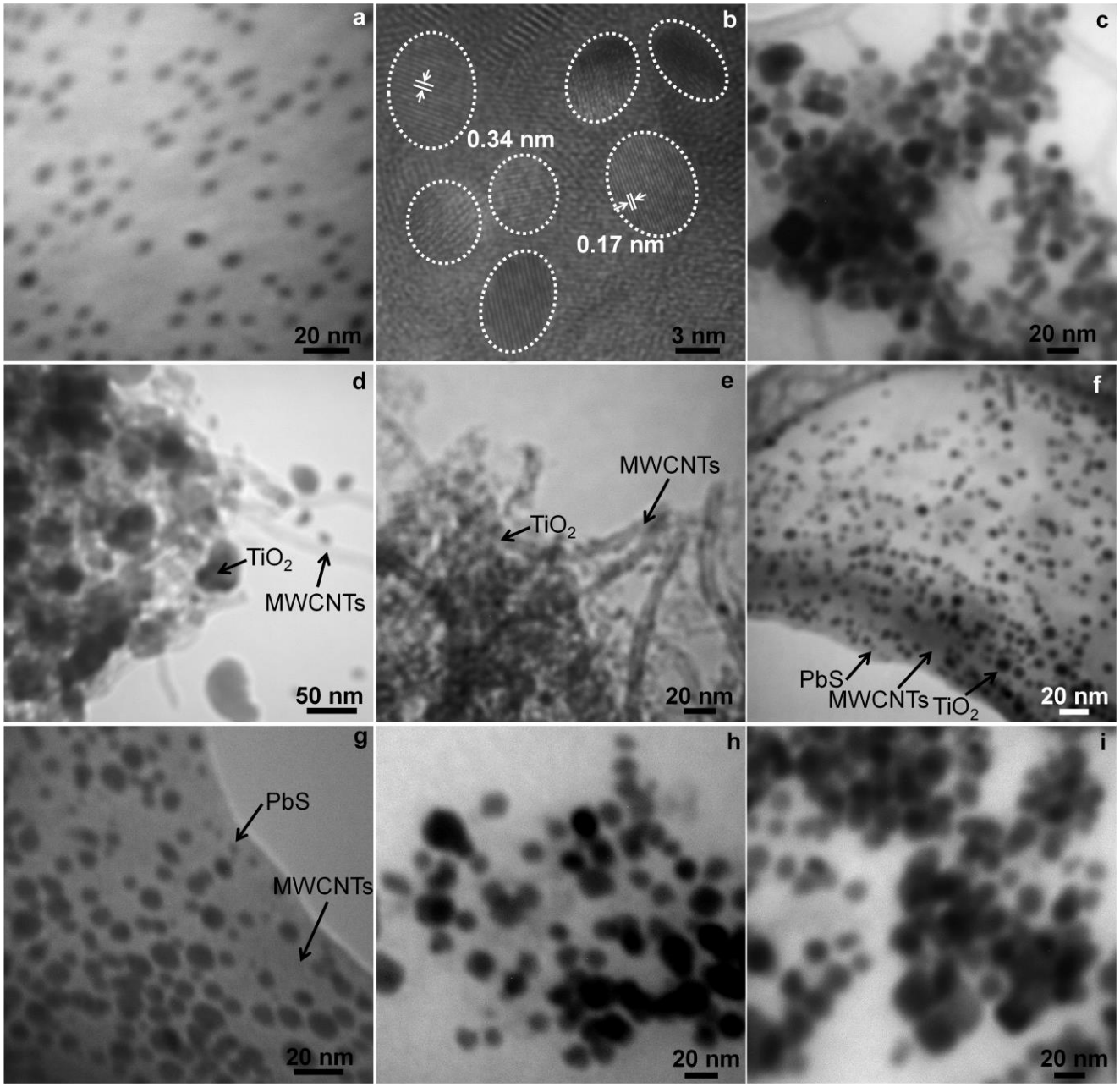

Figure 6 (a) TEM and (b) lattice scale images of PbS QDs. TEM images of (c) TiO_2, (d,e) TiO_2-MWCNTs, (f, g) TiO_2-MWCNTs/PbS and (h, i) SnS NPs.

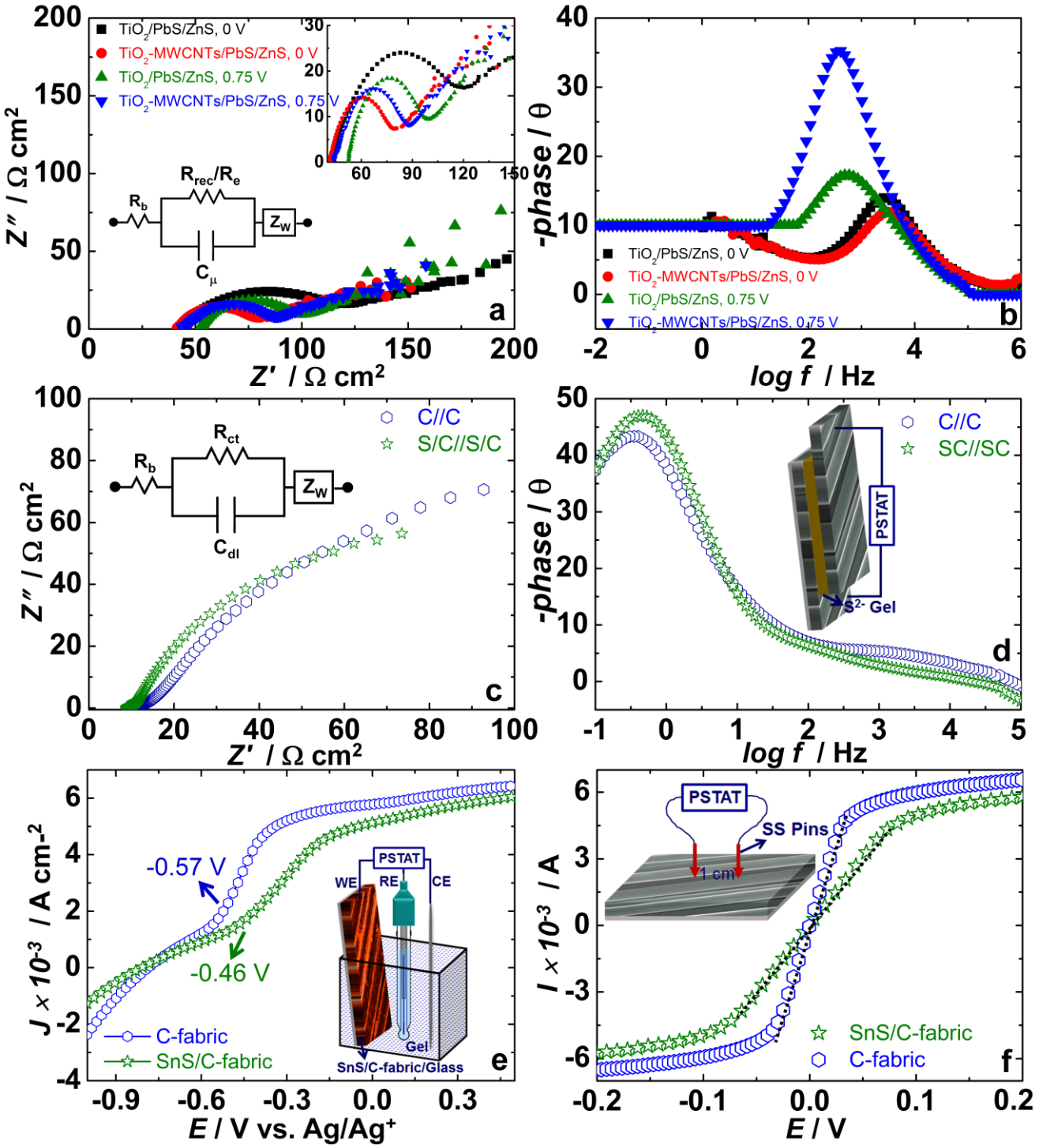

Figure 7 (a) Nyquist and (b) Bode plots of QDSCs with TiO_2/PbS/ZnS and TiO_2-MWCNTs/PbS/ZnS photoanodes, and SnS/C-fabric as the CE, and recorded under a white light irradiance of 30 mW cm^{-2}, and at dc potentials of 0.75 V and 0 V. (c) Nyquist and (d) Bode plots of symmetric cells with C-fabric and SnS/C-fabric (SC) electrodes. Respective equivalent circuits used for fitting the plots are shown as insets of (a) and (c). Insets of (d-f) show representative cell configurations used for the measurements.

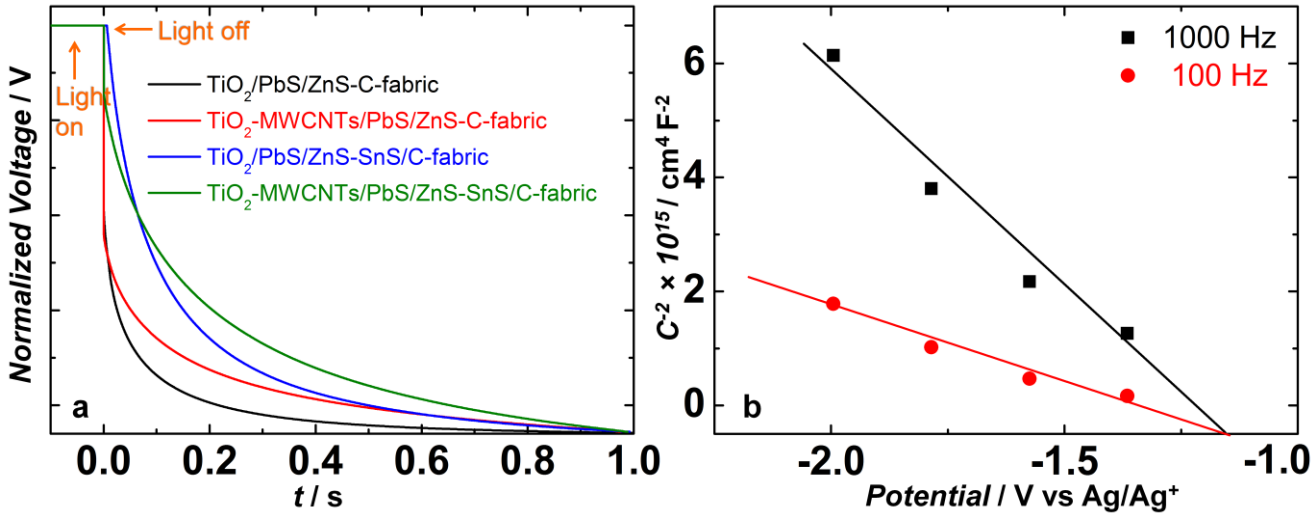

Figure 8 (a) Photovoltage *versus* time transients of QDSCs with the following photoanodes//counter electrode architectures: TiO_2/PbS/ZnS//C-fabric, TiO_2/PbS/ZnS//SnS/C-fabric, TiO_2-MWCNTs/PbS/ZnS//C-fabric and TiO_2-MWCNTs/PbS/ZnS//SnS/C-fabric, recorded under a white light irradiance of 30 mW cm^{-2}. (b) Mott-Schottky plots of the water based gel containing 10 wt% PVA, 0.1 M KCl, 0.1 mmol of TiO_2 NPs and 0.1 M Na_2S recorded with two Pt electrodes and an Ag/AgCl/KCl reference electrode.

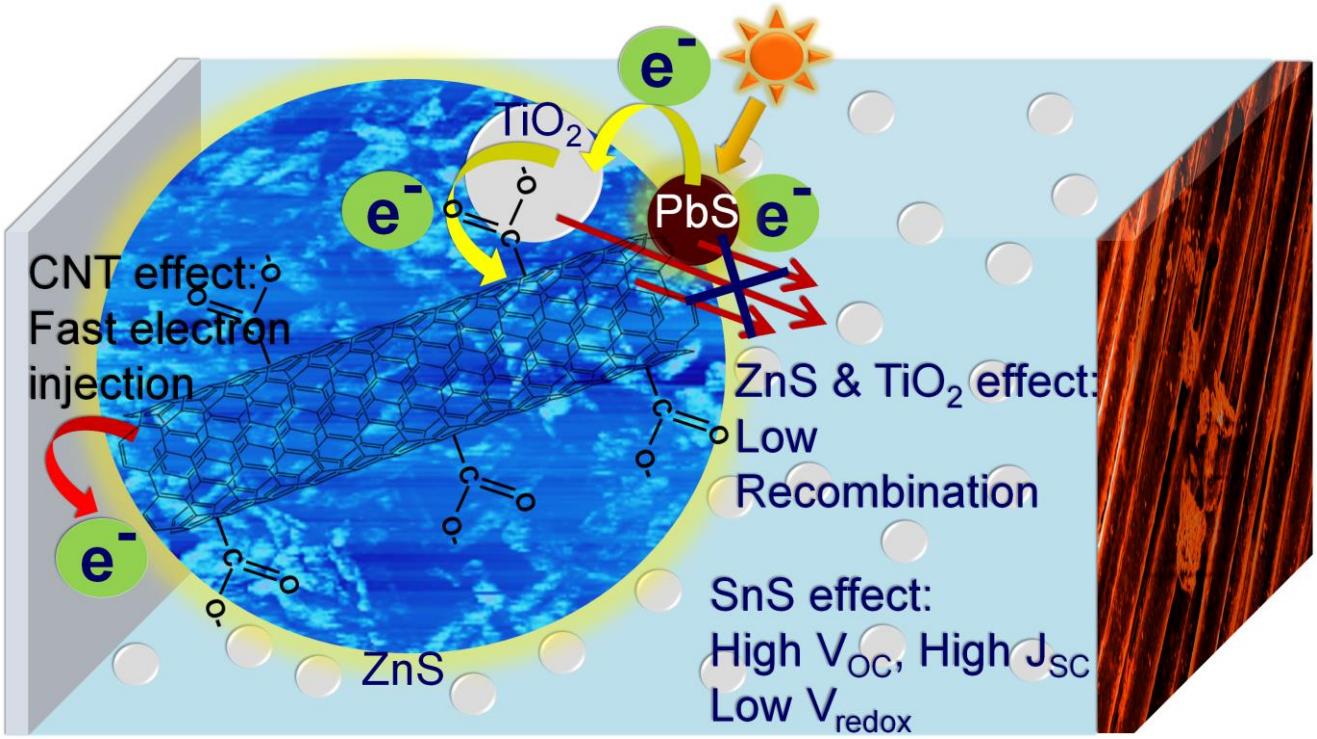

Graphical Abstract

Supporting Information

Effects of Carbon Nanotubes in Photoanode, Tin Sulfide in Counter Electrode and Titania in Electrolyte on Quantum Dot Solar Cell Performance

Ramesh K. Kokal, Melepurath Deepa, Ankarao Kalluri, Shristhi Singh, Isaac Macwan, Prabir K Patra, Jeff Gilarde*

Table S1 Solar cell parameters of cells by considering standard deviation, exposed cell area: 0.15 to 0.18 cm^2, under 1 sun illumination (AM 1.5, 100 mW cm^{-2}) with the listed photoanodes and counter electrodes.

Photoanode	Counter Electrode	V_{OC} (mV)	J_{SC} (mA cm^{-2})	FF(%)	η_{avg} (%)
TiO_2/PbS/ZnS	C-fabric	829.6 ± 1.7	11.42 ± 0.14	37.78 ± 1.22	3.58 ± 0.17
	SnS/C-fabric	877.4 ± 2.7	13.41 ± 0.41	35.7 ± 0.9	4.20 ± 0.25
TiO_2-MWCNTs/PbS/ZnS	C-fabric	832.1 ± 1.6	17.96 ± 0.35	35.33 ± 0.07	5.28 ± 0.13
	SnS/C-fabric	897.6 ± 2.4	19.72 ± 0.31	34.8 ± 0.2	6.16 ± 0.14

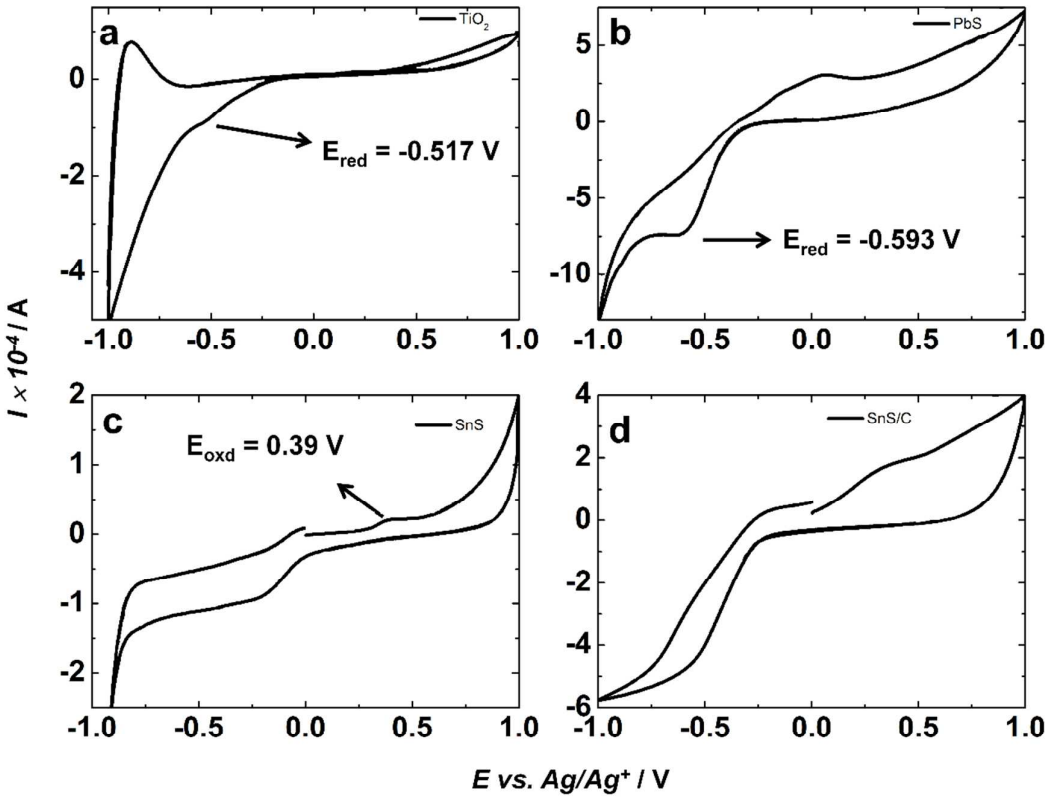

Figure S1 Cyclic voltammograms of (a) a pristine TiO_2 electrode, (b) a pristine PbS electrode, (c) a SnS/FTO electrode, and (d) a SnS/C-fabric electrode serving as working electrodes. All CV plots were recorded in a 0.1 M KCl solution as electrolyte, with a Pt sheet as the counter electrode and an Ag/AgCl/KCl as the reference electrode, at a scan rate of 10 mV s^{-1}.

Cyclic voltammograms of pristine- TiO_2, PbS, and SnS films (as working electrodes), recorded in an aqueous 0.1 M KCl solution, with a Pt rod as the counter electrode and a Ag/AgCl/KCl as the reference electrode are shown in Figure S1. For pristine TiO_2, a reduction peak was observed in the cathodic sweep at –0.517 V *versus* Ag/AgCl/KCl, and this E_{red} can be equated to the CB (conduction band) or LUMO (lowest unoccupied molecular orbital) position of TiO_2. The electrode potential of the reference is +0.197 V. So, E_{red} (*versus* NHE (normal hydrogen electrode)) of TiO_2 = –0.517 V + 0.197 V = –0.32 V. The value of

–0.32 V (*versus* NHE) in eV is given by: –4.5 eV (≅ 0 V *versus* NHE) – (–0.32V) = –4.18 ≅ –4.2 eV. The position of the valence band (VB) or HOMO (highest occupied molecular orbital) of TiO_2 is determined by addition of the pre-determined optical band gap energy value to the CB energy, i.e., –4.2 eV + (–3.11 eV) = –7.29 eV. For pristine PbS, a reduction peak was observed in the cathodic sweep at –0.593 V *versus* Ag/AgCl/KCl, and this E_{red} can be equated to the CB or LUMO (lowest unoccupied molecular orbital) position of CIS. So, E_{red} (*versus* NHE) of CIS = –0.593 V + 0.197 V = –0.396 V. The value of –0.396 V (*versus* NHE) in eV is given by: –4.5 eV – (–0.396V) = –4.1 eV. By adding the optical E_g of PbS to the CB energy level (–4.1 eV + (–1.09 eV)), the VB energy level is calculated to be at –5.19 ≅ –5.2 eV. For pristine SnS, a oxidation peak was observed in the anodic sweep at 0.39 V *versus* Ag/AgCl/KCl, and this E_{oxd} can be equated to the VB or HOMO (highest occupied molecular orbital) position of SnS. So, E_{oxd} (*versus* NHE) of SnS = 0.39 V + 0.197 V = 0.587 V. The value of 0.587 V (*versus* NHE) in eV is given by: –4.5 eV – (0.593V) = –5.08 ≅ –5.1 eV.

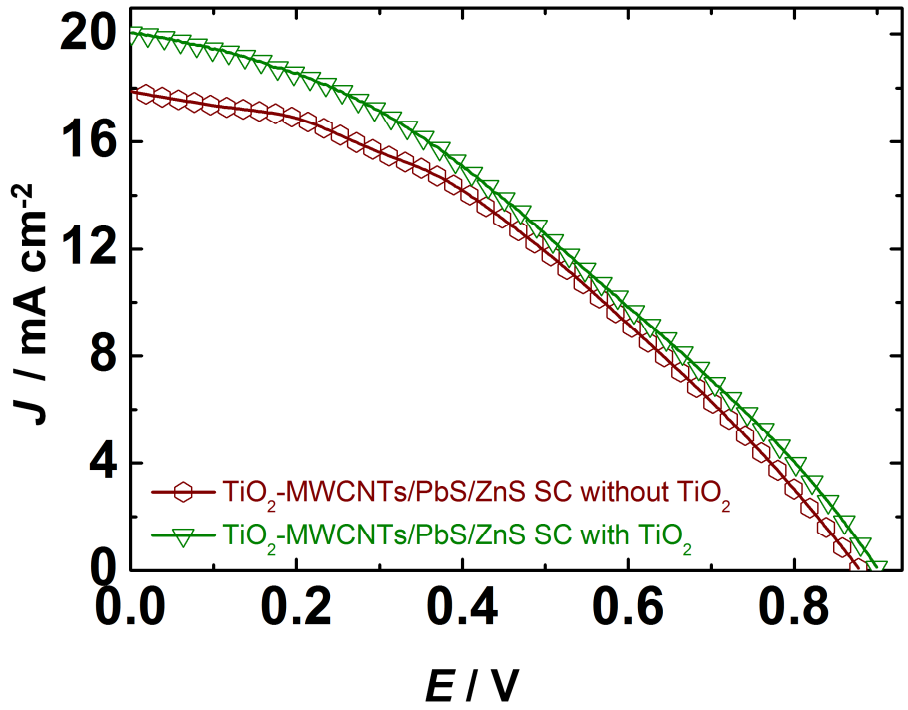

Figure S2 J-V characteristics of TiO_2-MWCNTs/PbS/ZnS-gel- SnS/C-fabric cells, with two different gels: one with 0.1 M Na_2S, 0.1 M KCl, 0.1 mmol TiO_2 NPs and 10 wt% of PVA in water, and the other without 0.1 mmol TiO_2 NPs.